An Abstract Of The Thesis Of

Stephen K. Crossno for the degree of Master of Science in Chemistry presented on June 16, 1997.

Title: Tetracalcium Lanthanide Borate Oxide: Structures and Optical Properties.

Abstract approved: Redacted for Privacy

Douglas A. Keszler

The main contribution of this work stems from the study of a series of borate oxides $Ca_4LnO(BO_3)_3$ containing calcium and a lanthanide (Ln). Crystal structures are described for the stoichiometric material $Ca_4EuO(BO_3)_3$ and two other alkaline-earth substituted analogs, $Ca_{1.76}Sr_{2.24}GdO(BO_3)_3$ and $Ca_{3.38}Mg_{0.62}GdO(BO_3)_3$. By analyzing crystal data from these materials as well as the lanthanide derivatives containing Sm, Eu, Gd, Tb, and Lu, relationships between BO_3-group orientations and second-order nonlinear optical susceptibilities are established. The results indicate that the magnetude of estimated susceptibility coefficients will increase for those materials which contain a smaller lanthanide atom and that this increase is primarily attributed to the BO_3-group reorientation that occurs as larger lanthanide atoms are replaced by smaller lanthanide atoms. Eu^{3+} luminescence for this series of materials is examined by using $Ca_4YO(BO_3)_3$ as the model host. VUV excitation spectra,

emission spectra, chromaticity data, brightness and lifetime measurements, and concentration quenching data are presented. Results suggest that the observed emission spectrum and calculated chromaticity values are directly related to the distorted octahedral geometry that surrounds the luminescent center. The material is shown to be an efficient red emitting phosphor. The level of brightness is approximately 50-60% relative to that of industrial standard $Eu^{3+}:Y_2O_3$.

Tetracalcium Lanthanide Borate Oxide: Structures and Optical Properties

by

Stephen K. Crossno

A THESIS

submitted to

Oregon State University

in partial fulfillment of
the requirements for the
degree of

Master of Science

Presented June 16, 1997
Commencement June 1998

Master of Science thesis of Stephen K. Crossno presented June 16, 1998

APPROVED:

Redacted for Privacy

Major Professor, representing Chemistry

Redacted for Privacy

Chair of Department of Chemistry

Redacted for Privacy

Dean of Graduate School

I understand that my thesis will become part of the permanent collection of Oregon State University libraries. My signature below authorizes release of my thesis to any reader upon request.

Redacted for Privacy

Stephen K. Crossno, Author

ACKNOWLEDGMENTS

This work was accomplished with the aid and support of many people. I am indebted to each of them.

To begin I recognize my major professor Doug Keszler to whom I am immeasurably grateful. Doug welcomed me into a group of distinguished students that later became a source of invaluable discussion and a library of helpful suggestions. Doug endeavored to present a host of fascinating research topics and was a constant source of guidance and information. Without his support, the work that follows in this dissertation and the subsequent completion of my graduate degree would not have been possible.

Next, I would like to extend thanks and appreciation to my colleagues, Ki-Seog Chang, Dr. Anthony Diaz, Dong Li, Greg Peterson, and Ken VandenBerghe. It has been my privilege to work with and learn from this outstanding group of scientists. I am honored to call them friends.

I would also like to express my deepest thanks for the efforts and sacrifices made by my parents, Annemie and Gary Crossno. Their love, encouragement, and devotion have been paramount in my strive towards excellence.

Additionally, it is my pleasure to thank Dr. Lee Kalbus. Without his assistance it is unlikely that I would have pursued an advanced degree. He has been a dear mentor and friend.

Finally, I thank my beloved wife and son who have journeyed along side me through the last three years. Together they have endured many trials and difficulties and yet have remained steadfast with their love and support.

CONTRIBUTING AUTHORS

VUV data were collected at the University of Georgia under the guidance of Dr. Richard Meltzer.

TABLE OF CONTENTS

LIST OF FIGURES

LIST OF FIGURES (Continued)

LIST OF TABLES

LIST OF APPENDIX TABLES

TETRACALCIUM LANTHANIDE BORATE OXIDE: STRUCTURES AND OPTICAL PROPERTIES

CHAPTER 1

Introduction

Research involving optical and luminescent materials during the last 30 years has lead to the development of many widely recognized uses. For example, laser applications encompass communications, image processing, computing, and medical surgery. With the aid of frequency conversion materials it is possible to exploit regions of the electromagnetic spectrum that would otherwise have been unavailable, thus, extending the utility of lasers. Light emitting solid-state materials have also found far-reaching applications that include various types of display technology, e.g., television and fluorescent lamps. Clearly, the investigation of new materials issues forth a means of replacing older, and less cost effective devices, with modern energy efficient ones, in addition to developing advanced technologies.

The work herein focuses on three aspects of the tetracalcium lanthanide (Ln) borate oxides [$Ca_4LnO(BO_3)_3$], a new series of materials. Motivation for this study is derived from structural characteristics that contribute to favorable optical and/or luminescent properties and their practical implications. To begin this study, the structures of three analogs to this series are determined in an effort to supplement the published crystal data on this group. Included here are two new

alkaline-earth, substituted isostructures. With the crystal structure data it is then possible to predict optical second-harmonic generation characteristics. Finally, Eu^{3+} luminescence properties are examined.

Optical Frequency Conversion:

The ability of crystalline nonlinear optical (NLO) materials to convert high-power laser light from one frequency to another (Figure 1.1) entails many important details. The power extracted from a second harmonic generating (SHG) crystal of length L, may be approximated by Eq. 1.1 (1),

$$P_{2\omega} \propto P_{\omega}^{2} \cdot L^{2} \cdot d_{jm}^{2} \exp(-L(\alpha_{\omega}+\tfrac{1}{2}\alpha_{2\omega})) \left[\frac{\sin^{2}L\cdot\Delta K/2}{(L\cdot\Delta K/2)^{2}}\right] \qquad [Eq.1.1]$$

where P_{ω} is the power of the incident beam, d_{jm} is the relevant SHG coefficient, α_{ω} is the absorption coefficient of the crystal at the fundamental wavelength, $\alpha_{2\omega}$ is the absorption coefficient of the crystal at the second harmonic wavelength, and ΔK is the wave vector mismatch between the fundamental and second harmonic waves. The exponential term approximates the absorption characteristics of the NLO crystal and the *sin* term describes the ability to phase match the incoming and doubled waves. It is evident from Equation 1.1 that large second harmonic coefficients may be desirable for producing high powers in the second harmonic wave. The second harmonic coefficient is defined as

$$d_{jm} \rightarrow \chi^{(2)}_{IJK}(\omega,\omega) = \frac{1}{V}\sum_{ijk} R_{Ii}\, R_{Jj}\, R_{Kk}\, \beta_{ijk}(\omega,\omega) \qquad [Eq.1.2]$$

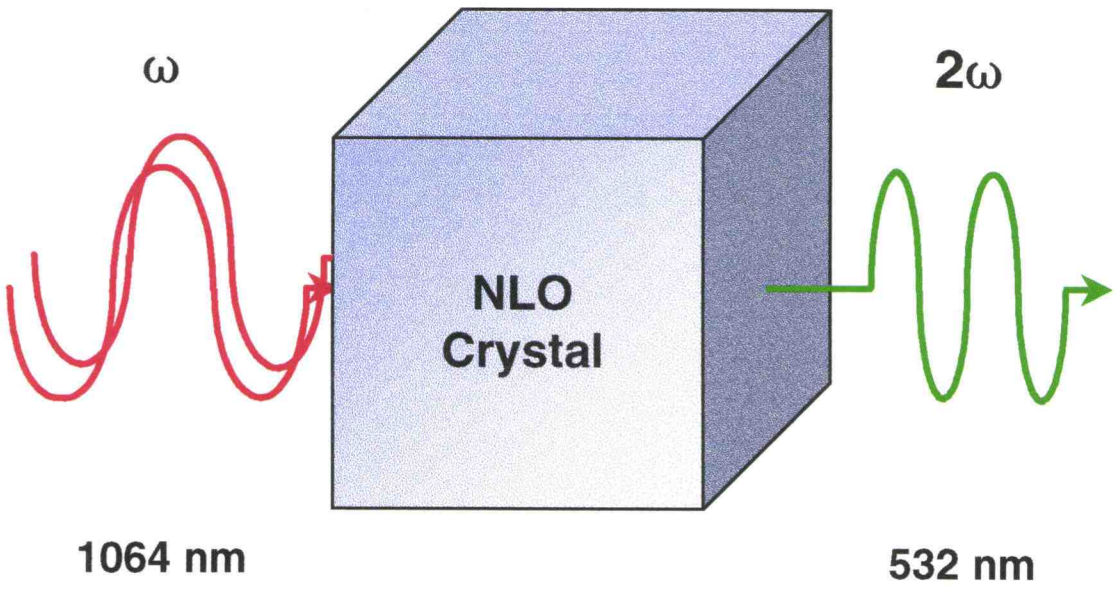

Figure 1.1 Frequency conversion of light via a crystalline medium.

where V is the volume of the unit cell, the R direction cosines relate molecular coordinates to crystal coordinates, and the $\beta_{ijk}(\omega,\omega)$ coefficients are the microscopic hyperpolarizability tensor components for the anionic groups under consideration.

$$\beta_{ijk}(\omega,\omega)=\frac{1}{4}h^2\sum_{P}\sum_{e,e'}\frac{\langle g|\hat{u}_i|e\rangle\langle e|\hat{u}_j|e'\rangle\langle e'|\hat{u}_k|g\rangle}{(\omega_e-\omega_g\omega-2\omega)(\omega'-\omega_g-\omega)} \qquad \textit{[Eq.1.3]}$$

In Equation 1.3, |g> represents a ground electronic state, and |e> and |e′> represent excited electronic states. The *ijk* subscripts on β can be 1, 2, or 3 (≡ *x, y,* or *z*) where *i* represents the direction of polarization induced by the incoming photons and the subscripts *j* and *k* indicate the directions of electric polarization for the incoming photons. For example, β_{333} refers to the magnitude of polarization induced in the *z* direction when two photons also polarized along *z* impinge on a molecule. Every possible interaction is described from a permutation over all possible *ijk* values. From Equation 1.2 it is noted that in order to maintain a large second harmonic coefficient the hyperpolarizability tensors must sum constructively. The material must be noncentrosymmetric, since a center of inversion requires each positive β_{ijk} to have a negative β_{ijk} of equal magnitude, resulting in a zero sum for Equation 1.2.

In addition to these requirements, a material must posses many other chemical and mechanical properties to be a useful frequency converter. For example, materials that melt congruently at relatively low temperatures are preferred, since, under these favorable growth conditions it can be easier to

obtain large, transparent crystals. Such crystals may also have greater optical quality, which, substantially increases their damage threshold. Conversion from materials having a wide transparency range spanning from the IR into the UV is also desirable.

Two borates, BBO and LBO, have been used commercially as frequency converters in the UV region (2). BBO has large nonlinear coefficients, 3 to 6 times that of the well-known converter KDP (3). The fifth harmonic generation of 1.06 μm Nd:YAG to 213 nm has been demonstrated in BBO with 11% overall efficiency (4). LBO exhibits a lower threshold power than BBO, and it has capabilities as an efficient frequency converter at high powers. LBO can achieve higher second harmonic efficiencies for mode-locked YAG lasers than KTP because of damage limitations in the latter crystals. LBO has the highest reported damage threshold of any commercially available solid-state frequency converter. Also, it has been shown to exhibit a threshold power for 50% conversion efficiency that is two orders of magnitude lower than that of KDP; it is optically transparent in the range of 160 nm to 2.6 μm, making it useful for applications in the UV region.

The favorable nonlinear properties of LBO are derived from the borate system of B_3O_7 rings. CLBO is also derived from this ring matrix and has been shown by powder SHG measurements and computations to be a promising NLO material (5, 6).

Eu^{3+} Luminescence:

The red luminescence of the Eu^{3+} ion doped into inorganic solids has been extensively studied (7-10). The sharp emission feature near 612 nm has found important applications in fluorescent lighting and display technologies such as color television and plasma displays. The emission transition occurs from the excited $^5D_0$ level to the ^7F_J levels (J=0,1,2,3,4,5,6) of the $4f^6$ configuration. A Eu^{3+} energy level diagram is drawn in Figure 1.2. Because f→f type transitions of the 4f orbitals are well shielded by the filled $5s^2$ and 5p ^{6}levels, these transitions are only weakly influenced by the host lattice. Furthermore, since the transitions are not spin allowed, long excited state lifetimes on the order of 10^{-3} seconds are observed.

In a centrosymmetric site, optical absorption transitions such as those for Eu^{3+} are strongly forbidden as electric-dipole transitions by the parity selection rule. Transitions can only occur, therefore, as weak magnetic-dipole transitions which obey the selection rule $\Delta J = 0, \pm 1$. However, the parity selection rule can be relaxed when odd components of the crystal field mix a small amount of opposite-parity wave functions (e.g., 5d) into the 4f wave functions. Such a case arises when the luminescent ion occupies a site that lacks or deviates from inversion symmetry to bring about the so-called forced electric-dipole transition. Transitions for $\Delta J = 0, \pm 2$ are hypersensitive to this effect (11,12).

For a luminescent center on a site of inversion, the most intense transition is $^5D_0 \rightarrow {}^7F_1$, which occurs near 590 nm. The orange color of this line is inadequate for display and lighting purposes. However, once the symmetry

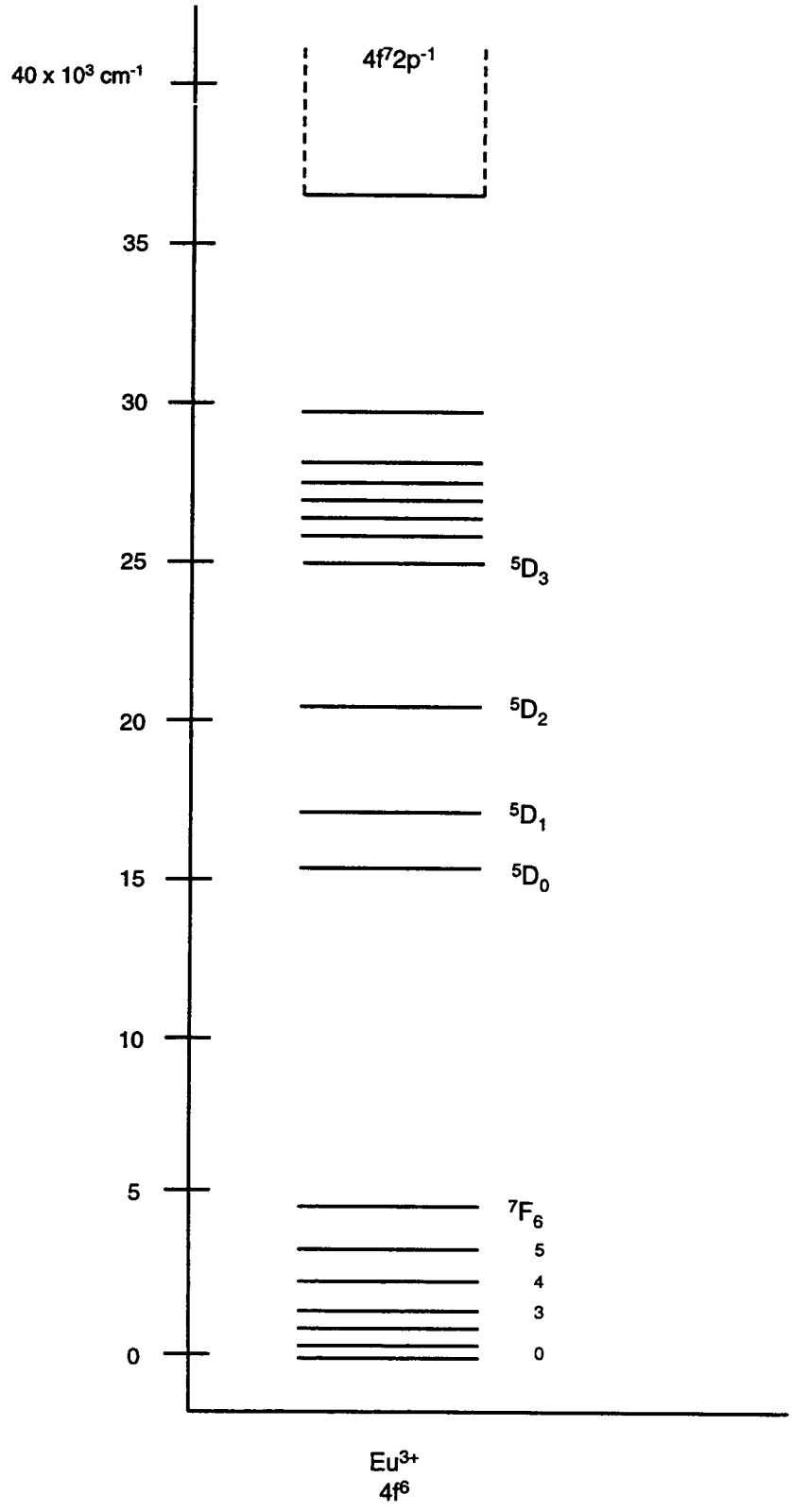

Figure 1.2 Energy level diagram for Eu^{3+} ion.

constraint is lifted, the $^5D_0 \rightarrow {}^7F_2$ transition can dominate, thereby, generating a saturated red line near 612 nm. The material $Eu^{3+}:Ca_4YO(BO_3)_3$ exhibits such a saturated red luminescence. Some of the characteristics of this emission are described in this work.

References:

1. M. J. Weber, *CRC Handbook of Laser Science and Technology*, "Section 1: Nonlinear Optical Materials", Boca Raton, Fla.: CRC Press, 1986.

2. G. Blasse, A. Bril, W. C. Nieuwpoort, *J. Phys. Chem. Solids.*, **27**, 1587-1592, (1966).

3. G. Blasse, *J. Solid State Chem.*, **4**, 52-54, (1972).

4. B. Saubat, C. Fouassier, P. Hagenmuller, *Mat. Res. Bull.*, **16**, 193-198, (1981).

5. G. A. West, N. S. Clements, *J. Luminescence*, **54**, 245-248, (1992).

6. B. R. Judd, *Phys. Rev.*, **127**, 750, (1966).

7. G. S. Ofelt, *J. Chem. Phys.*, **37**, 511, (1962).

CHAPTER 2

Structures and Optical Properties in the Borate Family $A_4LnO(BO_3)_3$ (A=Sr, Ca, Mg; Ln=lanthanide)

Stephen K. Crossno and Douglas A. Keszler

Oregon State University, Department of Chemistry

and Center for Advanced Materials Research

Corvallis, OR. 97331-4003

Inorganic Chemistry, manuscript in preparation

Abstract:

$Ca_4EuO(BO_3)_3$, $Ca_{1.76}Sr_{2.24}GdO(BO_3)_3$, and $Ca_{3.38}Mg_{0.62}GdO(BO_3)_3$ crystal structures are reported. The structural data of the tetracalcium lanthanide analogs (Sm, Eu, Gd, Tb, Lu) are used to investigate the relationship between BO_3-group orientation and the size of the lanthanide ion. This information is also used to calculate second-order optical susceptibility coefficients. Finally, the luminescence of Eu^{3+}-doped samples is reported.

Introduction:

Several physical properties must be incorporated into a single host material to produce a useful phosphor. Fluorescent lamp phosphors, for example, must have high photon emission following excitation at 185 and 254 nm, while a phosphor for a plasma display must exhibit a high brightness following 147 nm excitation. For these applications, the material should also have high UV and thermal stabilities. In displays and in some deluxe lamps, a red, green, and blue triplet of phosphors is used to produce selected colors or *white* light. The quality of the color from each phosphor is determined by its chromaticity coordinates, i.e., the location of the emission on a color map (1). Because of a strong and efficient saturated red emission at 612 nm, Eu^{3+}:Y_2O_3 is generally considered to set the standard for comparison with other red-emitting photoluminescent materials. In this work I will discuss the properties of Eu^{3+} doped into borate oxide hosts that are, in some ways, similar to those observed for Eu^{3+}:Y_2O_3. This discussion will include consideration of emission and vacuum ultraviolet excitation spectra, chromaticities, doping and brightness studies, concentration and thermal quenching, and particle morphology.

Recently, a class of materials $Ca_4LnO(BO_3)_3$ (Ln=lanthanide) related to the fluoride borate structure, $Ca_5F(BO_3)_3$ (2), was reported by Norrestam and Nygren (3). These materials are monoclinic, crystallizing in the noncentrosymmetric space group Cm. Several interesting characteristics of the structure should be considered in a continued investigation. Two structural features that affect the luminescent properties include an irregular octahedron around the lanthanide

and the interaction between the lanthanide and the nonborate bonded O^{2-} anion. Dirksen and Blasse have described Eu^{3+} luminescence in a doped sample of $Ca_4GdO(BO_3)_3$ (4). The study revealed a high energy charge transfer band, indicating a high quantum efficiency could be expected. The former has been attributed to the crystal structure, in which, the nonborate oxygen atom shared between Ca(1) and the lanthanide strongly couples with Eu^{3+} in the excited state. Support for the latter stems from weak Eu^{3+} intraconfigurational $4f^6$ excitation lines. The emission spectrum features an intense $^5D_0 \rightarrow {}^7F_2$ line at 612 nm, which, suggests that the material would be chromatically viable. Such a transition typically occurs in distorted octahedra since the activator site will deviate from inversion symmetry to yield a hypersensitive forced electric-dipole transition (5,6).

Additional interesting structural attributes of this structure type are the noncentrosymmetry and the relative orientations of the BO_3 groups. These features contribute to the second-order nonlinear optical properties recently reported for these materials (7). The structure type contains two crystallographically distinct types of BO_3 groups. One of these rests on a mirror plane of symmetry, and its orientation is unaffected by the nature of the Ln atom. The other BO_3 group, however, is free to reorient in response to the substitution of a small Ln atom for a large Ln atom. By examining all of the structural data that are now available, correlations among BO_3 group orientation, size of the Ln atom, and second-order optical nonlinear susceptibilities can be established.

Experimental:

Synthesis, Solid Solutions, Crystal Growth, and X-Ray Work

The materials $Ca_4LnO(BO_3)_3$ (Ln=Y, La, Eu, Gd) and $Ca_{4-x}A_xGdO(BO_3)_3$ (A=Sr, Mg) were prepared by conventional high-temperature techniques. Stoichiometric quantities of reagent grade $CaCO_3$, $Mg(NO_3)_2 \cdot 6H_2O$, $Sr(NO_3)_2$, B_2O_3, and the lanthanide oxides (Ln_2O_3) were used to prepare solid solutions and to grow single crystals. Materials having purities ≥ 99.99% were used to prepare all samples for luminescent studies. The reagents were initially ground together with a 5 mole% excess of B_2O_3 and decomposed at 800 °C for 1 h. The samples were again ground and fired at 1200 °C for an additional 8 h. Analysis of powder X-ray diffraction patterns obtained with a Philips automated diffractometer confirmed the formation of the desired product.

Structural analogs to $Ca_4GdO(BO_3)_3$ with Ca fully substituted by Mg, Sr, or Ba could not be produced. Approximate solubility limits for Sr and Mg were determined from cell refinements of powder X-ray data. These data were collected on an automated Philips diffractometer interfaced to a PC via a MetraByte DASH 8 data acquisition board. The peak positions were corrected by using NIST Si standard 640b. Unit-cell parameters were refined with the least-squares computer program POLSQ by using 15-20 peaks in the range $20 \leq 2\theta \leq 60°$. The results in Figure 2.1 indicate at least 50 and 25% of the Ca atoms can be replaced by Sr and Mg atoms, respectively. Further analyses beyond these limits were not undertaken

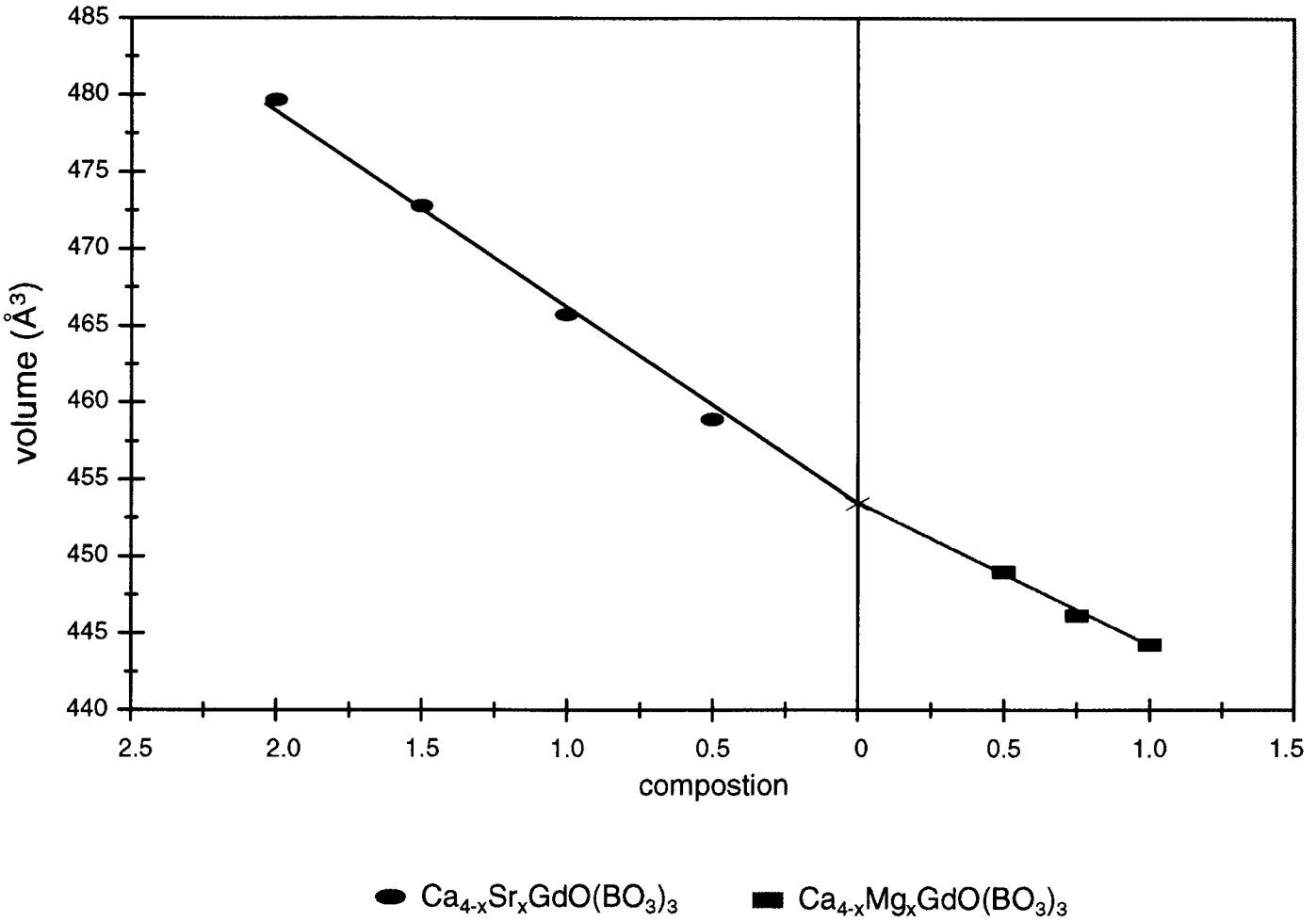

Figure 2.1 Solid solution of Sr and Mg substituted $Ca_4GdO(BO_3)_3$.

because of the poor quality of the diffraction data for those samples containing higher concentrations of Sr or Mg. Therefore, higher replacement of Ca may or may not occur.

Crystals of $Ca_4EuO(BO_3)_3$, $Ca_{1.76}Sr_{2.24}GdO(BO_3)_3$ and $Ca_{3.38}Mg_{0.62}GdO(BO_3)_3$ were obtained by melting the samples in Pt crucibles at 1300 °C for 1 h, followed by a cooling ramp at 4 °C/h to 1100 °C, and then a rapid cooling to room temperature. The latter two crystals were obtained from melts corresponding to the stoichiometric compositions $Ca_2Sr_2GdO(BO_3)_3$ and $Ca_3MgGdO(BO_3)_3$.

Small clear prismatic crystals with approximate dimensions 0.1 x 0.1 x 0.05 mm were mounted on glass fibers for collection of X-ray data. The data were collected on a Rigaku AFC6 diffractometer mounted on a rotating anode equipped with a graphite monochromator set for Mo Kα radiation. Unit-cell parameters were refined from 20 reflections in the range $30 \leq 2\theta \leq 36°$. In the case of $Ca_4EuO(BO_3)_3$ 1362 total reflections (1340 unique reflections) were measured to $2\theta_{max}=60°$ by using ω-2θ scans over the range of indices $-11 \leq h \leq 11$, $0 \leq k \leq 22$, and $-5 \leq l \leq 5$. For $Ca_{1.76}Sr_{2.24}GdO(BO_3)_3$, 2559 total reflections (1286 unique reflections) were measured to $2\theta_{max} = 75°$ over the range of indices $-14 \leq h \leq 14$, $0 \leq k \leq 27$, and $-6 \leq l \leq 6$, and 1963 total reflections (1884 unique reflections) were measured to $2\theta_{max} = 90°$ for $Ca_{3.38}Mg_{0.62}GddO(BO_3)_3$ with the range of indices $0 \leq h \leq 16$, $0 \leq k \leq 31$, and $-7 \leq l \leq 7$. A Digital μVax-II computer, together with programs from the TEXSAN crystallographic software package (8), was used to solve and refine the structure. The heavy atoms were

located by using the direct methods program MITHRIL (9) and previously reported structural results; positions of the other atoms were determined from analysis of difference electron density maps. Occupancies of the alkaline-earth sites in $Ca_{1.76}Sr_{2.24(8)}GdO(BO_3)_3$ were determined by constraining positional parameters and displacement coefficients on atoms Ca1 and Ca2 to those of atoms Sr1 and Sr2, respectively, and then refining multiplicities under the constraint of unit occupation of each site. The same procedure was used for the Mg analog with the parameters of the Mg site constrained to those of the Ca2 site. Following refinement of the model with isotropic displacement coefficients on each atom, the data were corrected for absorption with the program DIFABS (10).

In the case of $Ca_4EuO(BO_3)_3$, the Eu, Ca(1,2), B(2), and O(1,2,4,5) were refined with anisotropic displacement coefficients. The final cycle of full-matrix least-squares refinement with 1340 unique reflections having $F_o^2>3\sigma(F_o^2)$ and 76 parameters converged to R = 0.036 and R_w = 0.042. No atoms were refined with anisotropic displacement coefficients for $Ca_{1.76}Sr_{2.24}GdO(BO_3)_3$. The final refinement with 1286 observed reflections having $F_o^2>3\sigma(F_o^2)$ and 42 parameters converged to R = 0.067 and R_w = 0.084. For $Ca_{3.38}Mg_{0.62}GdO(BO_3)_3$, all atoms were refined anisotropically except the alkaline earth atoms Ca and Mg. Final refinement with 1876 unique reflections having $F_o^2>3\sigma(F_o^2)$ and 76 parameters converged to R = 0.039 and R_w = 0.052. Relevant crystal data for each of the structures is presented in Table 2.1. Final atomic coordinates and thermal parameters are listed in Tables 2.2-2.4, and selected interatomic distances and

associated angles are listed in Tables 2.5-2.7 and 2.8-2.10, respectively. Structural diagrams were drawn with the graphics program ATOMS (11).

Table 2.1 Crystallographic Data for $Ca_4EuO(BO_3)_3$, $Ca_{1.76}Sr_{2.24}GdO(BO_3)_3$, $Ca_{3.38}Mg_{0.62}GdO(BO_3)_3$.

	$Ca_4EuO(BO_3)_3$	$Ca_{1.76}Sr_{2.24(8)}GdO(BO_3)_3$	$Ca_{3.38(2)}Mg_{0.62}GdO(BO_3)_3$
Formula Weight, amu	504.70	615.53	500.53
Crystal System		Monoclinic	
Space Group		Cm [#8]	
a,Å	8.0983(8)	8.213(3)	8.061(2)
b,Å	16.034(3)	16.251(4)	15.943(3)
c,Å	3.567(4)	3.617(4)	3.540(2)
β	101.300(9)°	101.53(5)°	101.29(3)°
V,Å^3	454.2(1)	473.0(5)	446.2(3)
Z	2	2	2
D_{calc}, g cm^{-3}	3.690	4.248	3.678
F(000)	476	550	462
Diffracto-meter		Rigaku AFC6R	
Radiation		Mo Kα (λ=0.71069 Å) graphite-monochromated	
Data Collection	-11 ≤ h ≤ 11 0 ≤ k ≤ 22 -5 ≤ l ≤ 5	-14 ≤ h ≤ 14 0 ≤ k ≤ 27 -6 ≤ l ≤ 6	0 ≤ h ≤ 16 0 ≤ k ≤ 31 -7 ≤ l ≤ 7
No. Of Unique Obs. $F_o^2 \geq 3\sigma(F_o^2)$	1340	1286	1884
R	0.037	0.067	0.039
R_w	0.043	0.083	0.052

Table 2.2 Positional and Thermal parameters for $Ca_4EuO(BO_3)_3$.

$Ca_4EuO(BO_3)_3$	x	y	z	B^*_{eq}
Eu	0	0	0	0.49(2)
Ca1	0.3578(2)	0.1129(1)	-0.3287(4)	0.23(2)
Ca2	-0.2632(2)	0.1815(1)	-0.6561(4)	0.65(5)
O1	0.170(1)	0	-0.416(3)	0.6(3)
O2	-0.0890(7)	0.1426(4)	-0.078(2)	0.6(2)
O3	0.5320(7)	0.2310(4)	-0.278(2)	0.78(8)
O4	0.2053(8)	0.1721(4)	0.114(2)	1.0(2)
O5	0.5372(8)	0.0741(4)	-0.751(2)	0.7(2)
O6	-0.201(1)	0	-0.606(3)	0.5(2)
B1	-0.378(1)	0	-0.703(3)	0.2(1)
B2	0.049(1)	0.1955(6)	-0.085(3)	0.6(1)

$$*B_{eq}=(\frac{8\pi^2}{3})\sum_i \sum_i U_{ij}\ a_i^* a_j^* a_i \cdot a_j$$

atom	U_{11}	U_{22}	U_{33}	U_{12}	U_{13}	U_{23}
Eu	0.0061(2)	0.0066(2)	0.0059(2)	0	0.0011(1)	0
Ca2	0.0086(7)	0.0085(7)	0.0082(7)	0.0005(6)	0.0028(6)	0.0010(5)
O1	0.005(4)	0.008(4)	0.008(4)	0	0.001(3)	0
O2	0.008(3)	0.006(3)	0.010(3)	0.003(2)	0.001(2)	0.002(2)
O4	0.010(3)	0.015(3)	0.012(3)	0.009(2)	0.001(2)	0.000(2)
O5	0.012(3)	0.004(3)	0.011(3)	0.007(2)	0.001(2)	0.000(2)

Table 2.3 Positional and Thermal parameters for $Ca_{1.76}Sr_{2.24}GdO(BO_3)_3$

$Ca_{1.76}Sr_{2.24(8)}GdO(BO_3)_3$	x	y	z	B_{eq}
Gd	0	0	0	0.49(2)
Sr1†	0.3586(3)	0.1117(1)	-0.3280(7)	0.32(6)
Sr2‡	-0.2556(3)	-0.1805(1)	-0.6455(6)	0.40(6)
Ca1	0.3586	0.1117	-0.3280	0.32
Ca2	-0.2556	-0.1805	-0.6455	0.40
O1	0.173(3)	0	-0.411(7)	0.6(7)
O2	0.422(2)	0.360(1)	-0.078(4)	0.9(5)
O3	0.029(2)	0.268(1)	-0.271(4)	0.9(5)
O4	0.209(2)	0.171(1)	0.104(4)	1.1(5)
O5	0.035(2)	0.427(1)	0.250(5)	1.2(5)
O6	-0.203(3)	0	-0.602(7)	1.1(9)
B1	-0.378(1)	0	-0.69(1)	0.4(4)
B2	0.052(3)	0.194(1)	-0.079(7)	0.7(3)

†occupancy = 0.49(2)
‡occupancy = 0.63(2)

atom	U_{11}	U_{22}	U_{33}	U_{12}	U_{13}	U_{23}
Gd	0.0065(6)	0.0047(6)	0.0008(5)	0	0.0027(4)	0
O1	0.01(1)	-0.004(8)	0.02(1)	0	0.006(9)	0
O2	0.023(8)	0.005(6)	0.013(7)	0.003(6)	0.018(6)	0.004(5)
O3	0.019(8)	0.010(7)	0.011(7)	0.012(6)	0.014(6)	0.003(6)
O4	0.03(1)	0.015(7)	-0.002(6)	0.011(7)	0.004(6)	-0.003(5)
O5	0.019(8)	0.012(7)	0.014(8)	-0.014(7)	0.006(6)	-0.009(6)
O6	-0.006(8)	0.05(2)	0.00(1)	0	0.005(7)	0

Table 2.4 Positional and Thermal parameters for $Ca_{3.38}Mg_{0.62}GdO(BO_3)_3$

$Ca_{3.38(2)}Mg_{0.62}GdO(BO_3)_3$	x	y	z	B_{eq}
Gd	0	0	0	0.590(8)
Ca1	0.3579(1)	0.1128(6)	-0.3295(3)	0.57(1)
Ca2†	-0.2635(1)	0.1812(7)	0.3454(3)	0.5(1)
Mg	-0.2635	0.1812	0.3454	0.5
O1	0.1739(8)	0	-0.421(2)	0.6(1)
O2	-0.0873(6)	0.1430(3)	-0.080(1)	0.9(1)
O3	0.5297(7)	0.2306(3)	-0.277(2)	1.1(1)
O4	0.2067(6)	0.1718(4)	-0.887(2)	1.2(1)
O5	0.5357(7)	0.0743(3)	-0.752(5)	1.1(1)
O6	-0.205(1)	0	-0.607(2)	1.2(2)
B1	0.622(1)	0	-0.702(1)	0.5(2)
B2	0.0503(8)	0.1948(4)	0.918(7)	0.7(1)

†occupancy = 0.69(1)

atom	U_{11}	U_{22}	U_{33}	U_{12}	U_{13}	U_{23}
Gd	0.005(1)	0.0157(1)	0.0014(1)	0	-0.0012(6)	0
O1	0.002(2)	0.013(2)	0.007(2)	0	-0.002(2)	0
O2	0.010(1)	0.013(1)	0.011(2)	-0.005(1)	0.002(1)	0.001(2)
O3	0.019(2)	0.012(1)	0.013(2)	-0.002(1)	0.007(1)	-0.004(1)
O4	0.010(2)	0.022(2)	0.012(2)	0.006(1)	-0.002(1)	-0.000(1)
O5	0.018(2)	0.011(1)	0.014(2)	0.006(1)	0.002(1)	0.001(1)
O6	0.004(2)	0.037(4)	0.004(2)	0	-0.001(2)	0
B1	0.008(3)	0.006(2)	0.006(3)	0	-0.000(2)	0
B2	0.009(2)	0.011(2)	0.006(2)	0.003(2)	0.002(1)	0.000(1)

Table 2.5 Interatomic Distances (Å) for $Ca_4EuO(BO_3)_3$.

atoms	distance	atoms	distance
Eu-O1	2.21(1)	Ca2-O2	2.345(6)
-O1	2.26(1)	-O2	2.340(6)
-O2 x 2	2.397(6)	-O3	2.619(6)
-O6	2.44(1)	-O3	2.466(6)
-O6	2.35(1)	-O3	2.871(6)
Ca1-O1	2.344(6)	-O4	2.482(7)
-O3	2.348(6)	-O5	2.341(7)
-O4	2.385(6)	-O6	2.952(2)
-O4	2.327(6)	B1-O5 x 2	1.367(8)
-O5	2.372(6)	-O6	1.40(1)
-O5	2.359(6)	B2-O2	1.41(1)
		-O3	1.36(1)
		-O4	1.38(1)

Table 2.6 Interatomic Distances (Å) for $Ca_{1.76}Sr_{2.24}GdO(BO_3)_3$.

atoms	distance	atoms	distance
Gd-O1	2.25(2)	*M2-O2	2.43(1)
-O1	2.31(3)	-O2	2.36(2)
-O2 x 2	2.36(2)	-O3	2.84(2)
-O6	2.46(2)	-O3	2.71(2)
-O6	2.41(2)	-O3	2.57(2)
*M1-O1	2.35(1)	-O4	2.57(2)
-O3	2.39(2)	-O5	2.43(2)
-O4	2.38(2)	-O6	2.965(4)
-O5	2.38(2)	B1-O5 x 2	1.367(8)
-O5	2.39(2)	-O5	1.37(2)
		-O6	1.41(4)
		B2-O2	1.38(3)
		-O3	1.38(3)
		-O4	1.38(3)

*M1=Ca, Sr
*M2=Ca, Sr

Table 2.7 Interatomic Distances (Å) for $Ca_{3.38}Mg_{0.62}GdO(BO_3)_3$.

atoms	distance	atoms	distance
Gd-O1	2.237(8)	*M2-O2	2.323(5)
-O1	2.246(7)	-O2	2.345(5)
-O2 x 2	2.386(5)	-O3	2.462(5)
-O6	2.362(8)	-O3	2.610(6)
-O6	2.441(7)	-O3	2.848(6)
Ca1-O1	2.313(4)	-O4	2.479(6)
-O3	2.320(5)	-O5	2.329(6)
-O4	2.307(5)	-O6	2.927(2)
-O4	2.362(6)	B1-O5 x 2	1.369(6)
-O5	2.337(5)	-O6	1.37(1)
-O5	2.347(6)	B2-O2	1.384(8)
		-O3	1.368(8)
		-O4	1.364(8)

*M2=Ca, Mg

Table 2.8 Bond Angles (°) for $Ca_4EuO(BO_3)_3$.

O1-Eu-O1	105.7(4)	O1-Ca1-O5	100.1(3)
O1-Eu-O2	97.8(1)	O1-Ca1-O5	100.6(3)
O1-Eu-O2	102.8(1)	O3-Ca1-O4	86.9(2)
O1-Eu-O4	73.1(2)	O3-Ca1-O4	90.5(2)
O1-Eu-O4	71.1(1)	O3-Ca1-O5	80.1(2)
O1-Eu-O6	78.6(4)	O3-Ca1-O5	83.5(2)
O1-Eu-O6	79.5(4)	O4-Ca1-O4	98.4(2)
O1-Eu-O6	174.8(4)	O4-Ca1-O5	80.6(2)
O1-Eu-O6	175.7(4)	O4-Ca1-O5	81.5(2)
O2-Eu-O2	145.1(3)	O4-Ca1-O5	170.4(2)
O2-Eu-O4	48.0(2)	O4-Ca1-O5	170.5(2)
O2-Eu-O4	166.5(2)	O5-Ca1-O5	97.9(2)
O2-Eu-O6	76.3(1)	O2-Ca2-O2	99.2(2)
O2-Eu-O6	80.9(1)	O2-Ca2-O3	54.1(2)
O6-Eu-O6	96.2(4)	O2-Ca2-O3	83.2(2)
O4-Eu-O4	118.8(2)	O2-Ca2-O3	84.2(2)
O4-Eu-O6	109.1(1)	O2-Ca2-O3	87.6(2)
O4-Eu-O6	110.7(1)	O2-Ca2-O3	173.1(2)
O6-Eu-O6	96.2(4)	O2-Ca2-O3	176.4(2)
O1-Ca1-O3	175.7(3)	O2-Ca2-O4	94.3(2)
O1-Ca1-O4	88.9(3)	O2-Ca2-O4	123.2(2)
O1-Ca1-O4	89.4(3)	O2-Ca2-O5	101.3(2)

Table 2.8 Cont.

O2-Ca2-O6	67.6(3)	O3-Ca2-O5	78.3(2)
O2-Ca2-O6	70.1(2)	O3-Ca2-O5	156.3(2)
O3-Ca2-O3	89.1(2)	O3-Ca2-O6	109.7(2)
O3-Ca2-O3	125.5(1)	O3-Ca2-O6	114.1(2)
O3-Ca2-O3	100.0(2)	O3-Ca2-O6	115.0(2)
O3-Ca2-O4	55.0(2)	O4-Ca2-O5	128.6(2)
O3-Ca2-O4	73.5(2)	O4-Ca2-O6	163.2(3)
O3-Ca2-O4	80.8(2)	O5-Ca2-O6	52.2(2)
O3-Ca2-O5	78.2(2)		

Table 2.9 Bond Angles (°) for $Ca_{1.76}Sr_{2.24}GdO(BO_3)_3$.

O1-Gd-O1	104.8(9)	O1-M1-O5	100.0(7)
O1-Gd-O2 (X2)	96.5(4)	O3-M1-O4	86.2(6)
O1-Gd-O2 (X2)	102.3(4)	O3-M1-O4	88.9(6)
O1-Gd-O4 (X2)	71.4(4)	O3-M1-O5	81.6(6)
O1-Gd-O4 (X2)	71.8(4)	O3-M1-O5	84.2(6)
O1-Gd-O6	79.7(9)	O4-M1-O4	99.0(6)
O1-Gd-O6	79.8(9)	O4-M1-O5	80.3(5)
O1-Gd-O6	175.5(8)	O4-M1-O5	80.5(6)
O1-Gd-O6	175.5(9)	O4-M1-O5	170.4(6)
O2-Gd-O2	148.1(9)	O4-M1-O5	170.5(7)
O2-Gd-O4 (X2)	46.8(5)	O5-M1-O5	98.6(6)
O2-Gd-O4 (X2)	164.1(5)	O2-M*2-O2	97.9(7)
O2-Gd-O6 (X2)	76.9(4)	O2-M2-O3	54.5(5)
O2-Gd-O6 (X2)	82.4(4)	O2-M2-O3	84.3(5)
O4-Gd-O4	117.7(6)	O2-M2-O3	85.6(6)
O4-Gd-O6 (X2)	110.1(4)	O2-M2-O3	90.2(5)
O4-Gd-O6 (X2)	110.5(4)	O2-M2-O3	171.9(6)
O6-Gd-O6	95.8(8)	O2-M2-O3	176.5(5)
O1-M*1-O3	175.3(6)	O2-M2-O4	94.0(5)
O1-M1-O4	89.5(7)	O2-M2-O4	125.3(5)
O1-M1-O4	89.7(7)	O2-M2-O5	101.5(6)
O1-M1-O5	99.9(7)	O2-M2-O5	103.1(5)

Table 2.9 Cont.

O2-M2-O6	67.5(6)	O3-M2-O5	77.2(5)
O2-M2-O6	70.4(6)	O3-M2-O5	157.5(5)
O3-M2-O3	86.3(5)	O3-M2-O6	111.8(5)
O3-M2-O3	99.9(4)	O3-M2-O6	113.8(6)
O3-M2-O3	125.6(3)	O3-M2-O6	114.6(6)
O3-M2-O4	53.5(5)	O4-M2-O5	126.4(6)
O3-M2-O4	74.1(5)	O4-M2-O6	162.0(6)
O3-M2-O4	80.7(5)	O5-M2-O6	52.1(5)
O3-M2-O5	76.8(5)		

*M1=Ca, Sr
*M2=Ca, Sr

Table 2.10 Bond Angles (°) for $Ca_{3.38}Mg_{0.62}GdO(BO_3)_3$.

O1-Gd-O1	104.3(3)	O1-M1-O5	100.7(2)
O1-Gd-O2 (X2)	97.4(1)	O3-M1-O4	86.9(2)
O1-Gd-O2 (X2)	103.0(1)	O3-M1-O4	90.1(2)
O1-Gd-O4 (X2)	70.6(1)	O3-M1-O5	80.4(2)
O1-Gd-O4 (X2)	72.8(1)	O3-M1-O5	83.6(2)
O1-Gd-O6	79.6(3)	O4-M1-O4	98.6(2)
O1-Gd-O6	81.1(3)	O4-M1-O5	80.3(2)
O1-Gd-O6	174.5(2)	O4-M1-O5	81.3(2)
O1-Gd-O6	176.1(3)	O4-M1-O5	170.4(2)
O2-Gd-O2	145.6(2)	O4-M1-O5	170.5(2)
O2-Gd-O4 (X2)	47.9(1)	O5-M1-O5	98.2(2)
O2-Gd-O4 (X2)	165.9(1)	O2-*M2-O2	98.7(2)
O2-Gd-O6 (X2)	76.2(1)	O2-M2-O3	53.8(1)
O2-Gd-O6 (X2)	81.1(1)	O2-M2-O3	83.0(2)
O4-Gd-O4	118.3(2)	O2-M2-O3	84.5(2)
O4-Gd-O6 (X2)	109.6(1)	O2-M2-O3	88.4(2)
O4-Gd-O6 (X2)	111.0(1)	O2-M2-O3	172.8(2)
O6-Gd-O6	95.0(3)	O2-M2-O3	176.6(2)
O1-*M1-O3	175.8(2)	O2-M2-O4	93.7(2)
O1-M1-O4	88.9(2)	O2-M2-O4	122.8(2)
O1-M1-O4	90.2(2)	O2-M2-O5	101.9(2)
O1-M1-O5	99.4(2)	O2-M2-O5	103.0(2)

Table 2.10 Cont.

O2-M2-O6	68.1(2)	O3-M2-O5	77.8(2)
O2-M2-O6	70.7(2)	O3-M2-O5	156.8(2)
O3-M2-O3	88.5(2)	O3-M2-O6	110.6(2)
O3-M2-O3	100.1(1)	O3-M2-O6	113.7(2)
O3-M2-O3	125.6(1)	O3-M2-O6	114.5(2)
O3-M2-O4	55.3(2)	O4-M2-O5	128.5(2)
O3-M2-O4	73.0(1)	O4-M2-O6	163.0(2)
O3-M2-O4	81.1(2)	O5-M2-O6	52.1(2)
O3-M2-O5	77.6(2)		

* M2=Ca, Mg

Optical Measurements

Emission spectra were obtained by using a spectrofluorimeter equipped with Cary excitation and Oriel emission monochromators and an Oriel 350-W Xe lamp as the source (Fig. 2.2). Emission spectra were corrected for variation in PMT response and the wavelength-dependent throughput of the monochromator. Integrated emission intensities were determined by irradiating samples at 254 nm with an Oriel Hg pen lamp; the emission was passed through a UV filter and measured with a Hamamatsu PMT in combination with a Keithley picoammeter (Fig. 2.3). VUV excitation spectra were obtained at the University of Georgia. Variable temperature luminescence lifetime measurements were made from 4.2 to 298 K by irradiating samples mounted in a Cryo Industries helium flow cryostat with the fourth harmonic (266 nm) of a pulsed Molectron Nd:YAG laser (pulse width = 10 ns; see Fig 2.4).

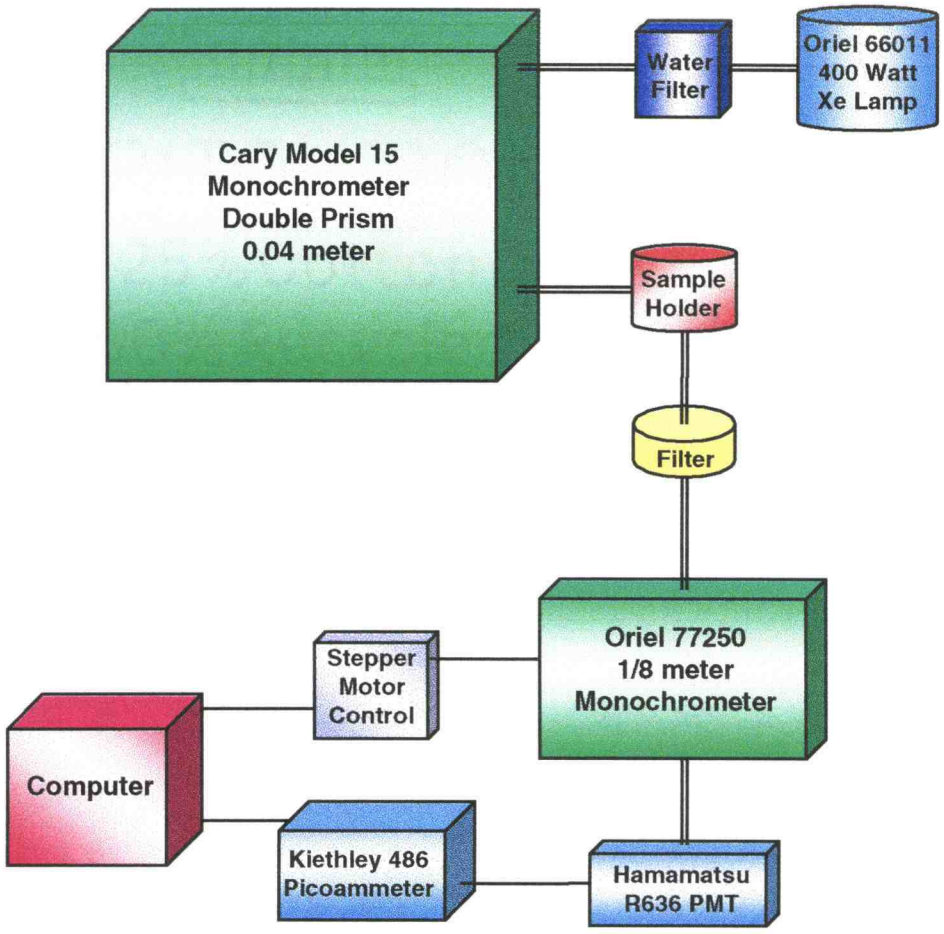

Figure 2.2 Spectometer diagram.

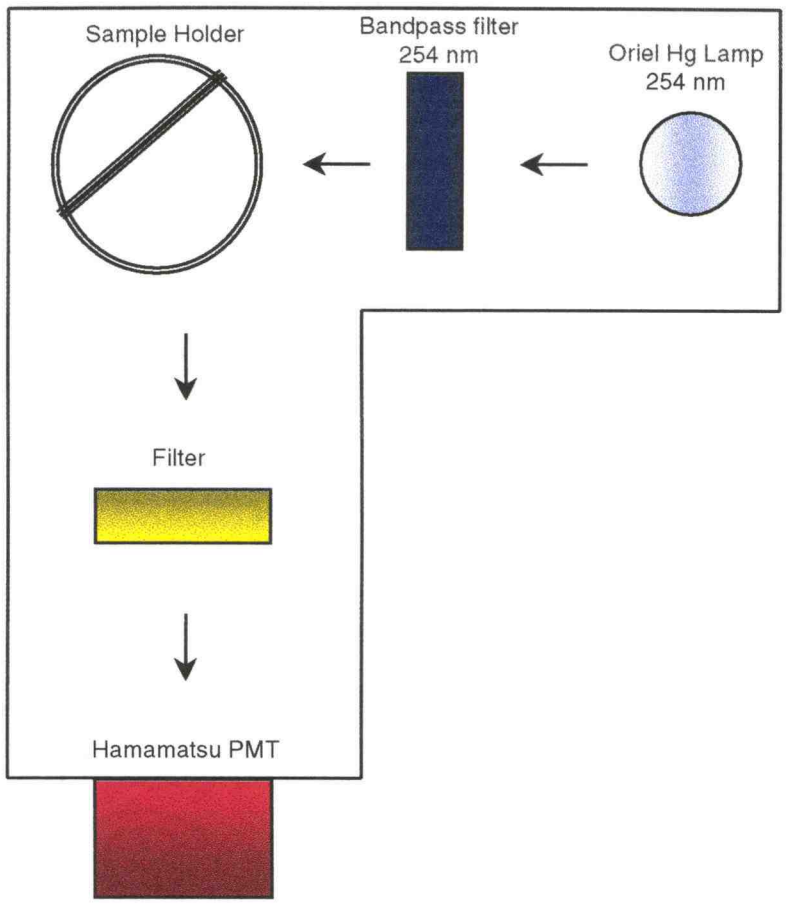

Figure 2.3 Diagram of apparatus used in brightness measurments.

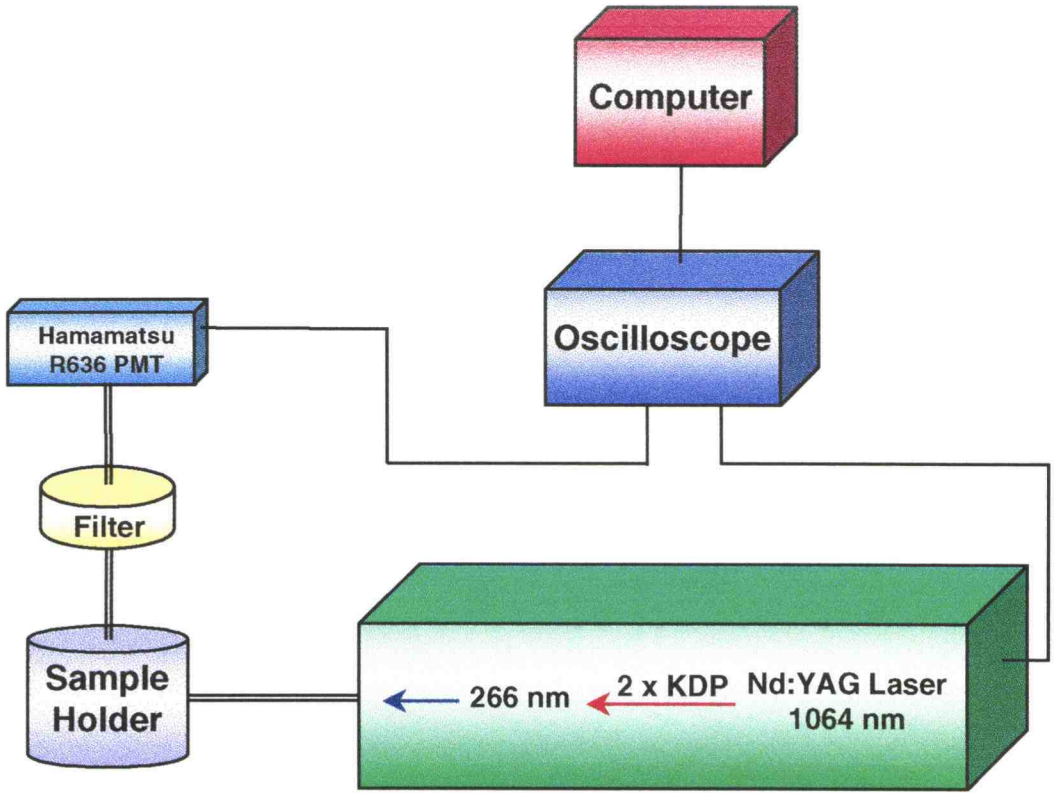

Figure 2.4 Diagram of apparatus used in lifetime measurements.

Results and Discussion:

Crystal Structure of $Ca_4EuO(BO_3)_3$

The unit-cell contents of $Ca_4EuO(BO_3)_3$ are depicted in Figure 2.5. It is isostructural to the Sm analog reported by Norrestam and Nygren (3) and to the Gd, Tb, and Lu analogs reported by Ilyukhin (12). It should be noted that no disorder between the alkaline-earth and lanthanide atom sites was detected upon refinement of the site multiplicities. A fragment demonstrating the connectivity of the metal-centered environments is shown in Figure 2.6. The O octahedron around Eu is irregular with bond distances ranging from 2.21(1) to 2.44(1) Å. Two additional interactions with the O(4) atom at 3.207(1) Å, however, may indicate a weak Eu-O interaction and a 6+2 coordination. Bond-valence sums produce a Eu valence of 2.929 for the 6-coordinate site and a valence of 3.072 for the 8-coordinate environment. Since each long Eu-O interaction represents only 15% of the electron density associated with the short distances, a description of the environment about the Eu atom as a highly distorted octahedron is favored.

Two pairs of Ca-centered distorted octahedra share three triangular borate groups with the Eu-centered octahedron. A mirror plane that bisects the lanthanide and B(1) sites perpendicular to the *b* axis relates the two pairs. The Ca(1)-centered octahedron is more regular than that surrounding the Eu ion and has bond distances that range from 2.327(6) to 2.385(6) Å. Like Eu, Ca(2) exhibits an irregular octahedron with bonds ranging from 2.340(6) to 2.952(2) Å. In this case, however, bond valence calculations reveal that the two additional

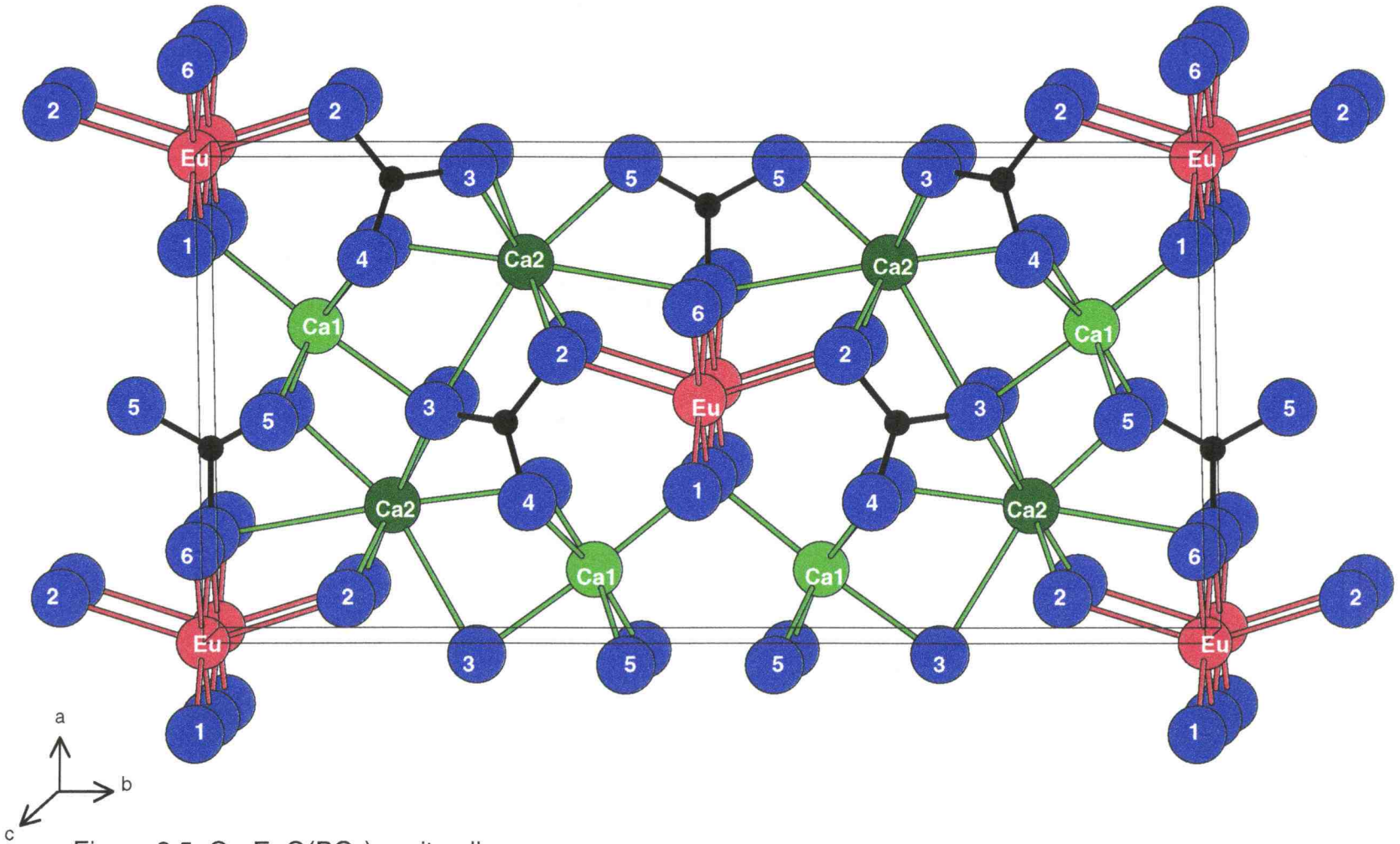

Figure 2.5 $Ca_4EuO(BO_3)_3$ unit cell.

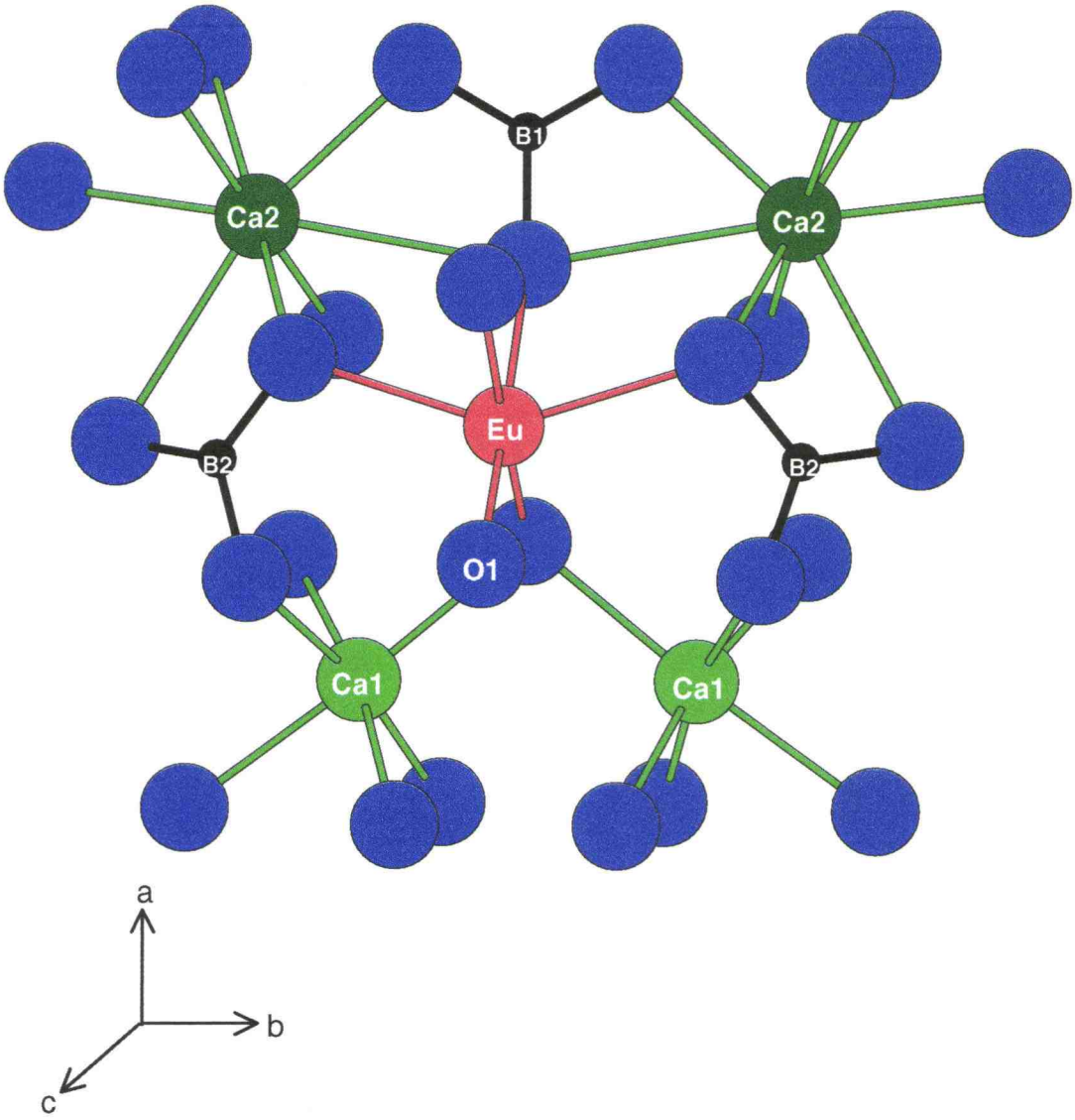

Figure 2.6 Fragment of the $Ca_4EuO(BO_3)_3$ structure, showing atomic labeling of the atoms and the metal-oxygen bonds.

bonding interactions to O(3,6) make the site 8 coordinate. 1.769 is the valence sum for Ca(2) in a 6 coordinate site, while, the expected 2^+ oxidation is more closely approached by 1.925 with Ca(2) in an 8 coordinate site. The corresponding Ca-O bond distances are 2.871(6) and 2.952(2) Å.

Crystal Structures of $Ca_{1.76}Sr_{2.24}GdO(BO_3)_3$ and $Ca_{3.38}Mg_{0.62}GdO(BO_3)_3$

The alkaline earth substituted materials $Ca_{1.76}Sr_{2.24(8)}GdO(BO_3)_3$ and $Ca_{3.38(2)}Mg_{0.62}GdO(BO_3)_3$ are isostructural with the parent material $Ca_4GdO(BO_3)_3$. The Sr analog exhibits the predicted expansion of the unit-cell parameters and the Mg analog exhibits a corresponding contraction (Fig. 2.1). Refinement of the Ca-Sr multiplicity parameters resulted in a random distribution between the two Ca sites. Multiplicity refinement of the Ca-Mg analog showed Mg substitution to occur exclusively on the Ca(2) site. This was later confirmed by bond valence calculations on the O(1) site. Whether the site occupancy is totally Ca or Mg a bond valence sum of 2.05 is obtained. This could only occur with Mg on the Ca(2) site since there is no connection to O(1).

BO_3-group Orientation

The 3-coordinate borate groups appear to be in the same plane as viewed down [001] in Figure 2.7. As illustrated in Figure 2.8, however, each vector normal of the B(2) triangles is tilted off the *c* axis. Since, the B(1)-centered triangles are located on special positions, only the B(2)-centered triangles undergo slight shifts as the lanthanide is changed in the series Sm, Eu, Gd, Tb,

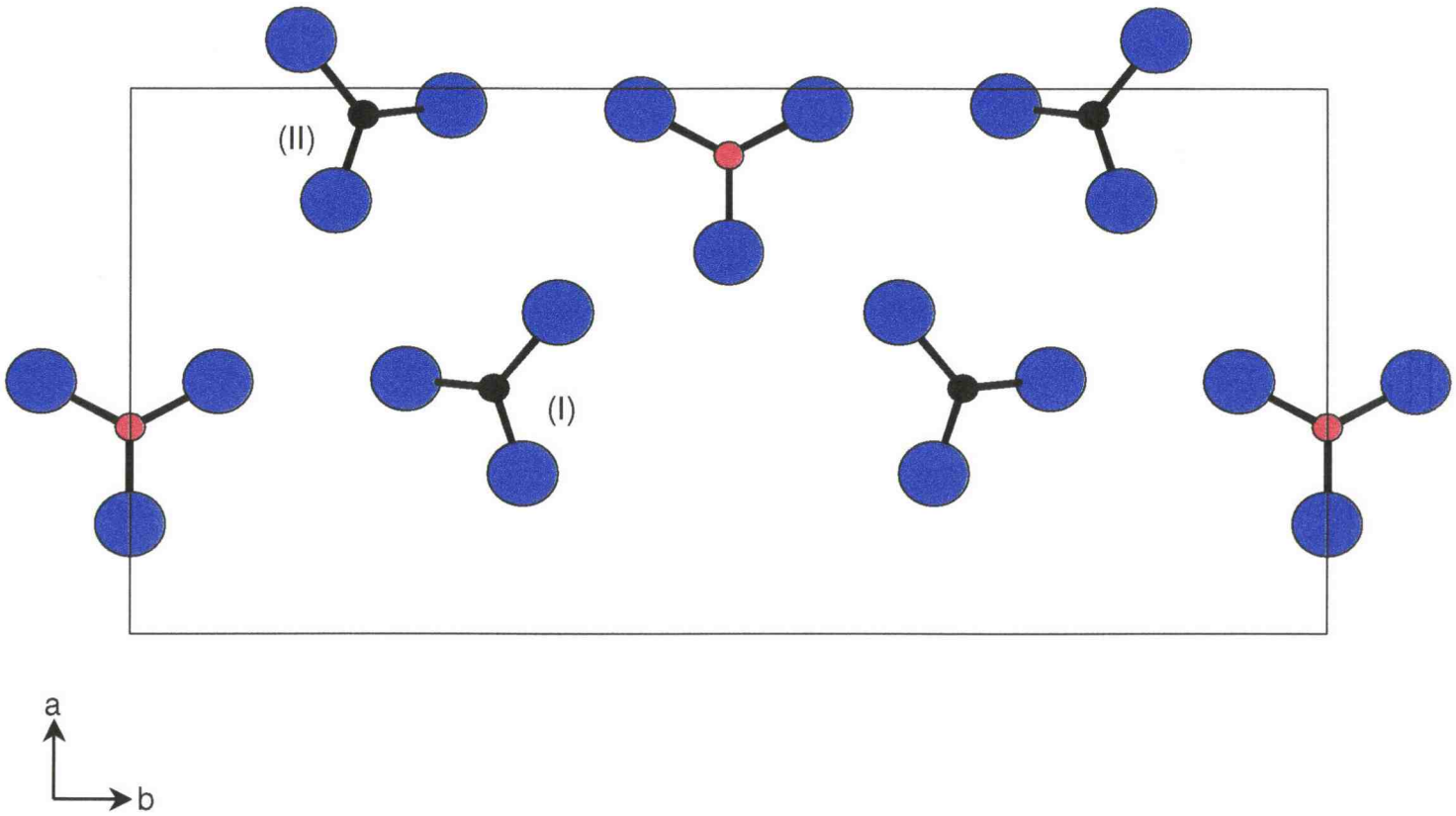

Figure 2.7 Borate triangles from the $Ca_4EuO(BO_3)_3$ unit cell as viewed down the 001.

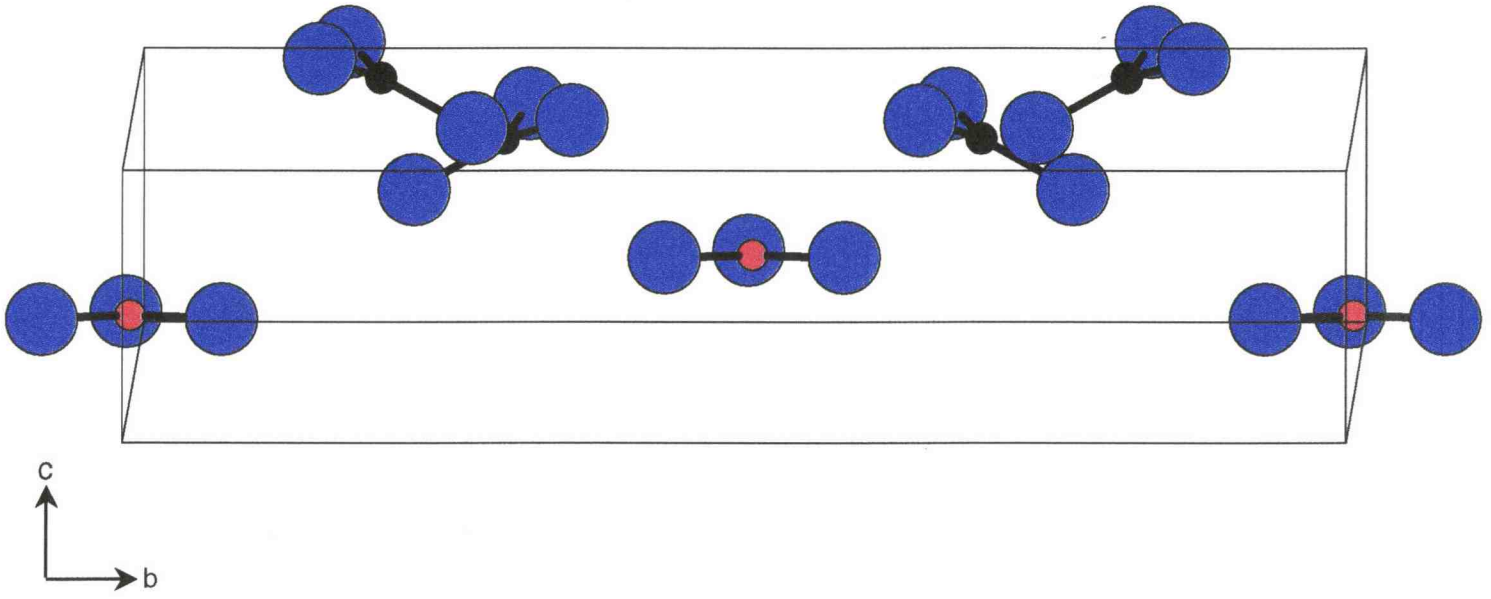

Figure 2.8 Borate triangles from $Ca_4EuO(BO3)_3$ unit cell as viewed down the 100 plane.

and Lu. A program written in this laboratory was employed to compute the orientations of the B(2) triangles for comparison with calculated nonlinear optical susceptibility coefficients. The program code is outlined in Appendix 2.

Calculation of the orientation of the BO_3 triangles entails four rudimentary steps: (1) converting the crystal system axes into Cartesian axes, (2) establishing a plane within the system from the three oxygen atom positions in a BO_3 group, (3) determination of that planes' normal vector, and (4) calculation of the angle between the normal vector and each of the Cartesian axes. Although, the final information represents angles in the Cartesian system, any structural trend that develops is also applicable to the crystal system. The calculation described has been performed on the BO_3 groups labeled (I) and (II) in Figures 2.7-2.8. Plots of the calculated angles against the ratio of the alkaline-earth to lanthanide radii are illustrated in Figures 2.9-2.10. The calculated slopes are given in Table 2.11 together with the corresponding angles.

Table 2.11 Angles and slopes for B(2) triangle groups (I) and (II).

	Group (I)			Group (II)		
RE	N*-a	N-b	N-c	N-a	N-b	N-c
Sm	46.04	81.71	45.45	73.22	29.22	66.82
Eu	45.91	81.82	45.33	73.15	29.04	67.23
Gd	45.85	82.11	45.23	73.10	28.85	67.35
Tb	45.81	82.50	45.07	73.09	28.61	67.650
Lu	45.71	83.59	45.01	72.81	28.13	68.44
slope	-1.925	15.24	-3.172	-3.113	-8.252	11.97
R^2	0.6379	0.9878	0.7303	0.9858	0.9366	0.9549

(N*-a) angle between normal vector and *a*-axis etc.

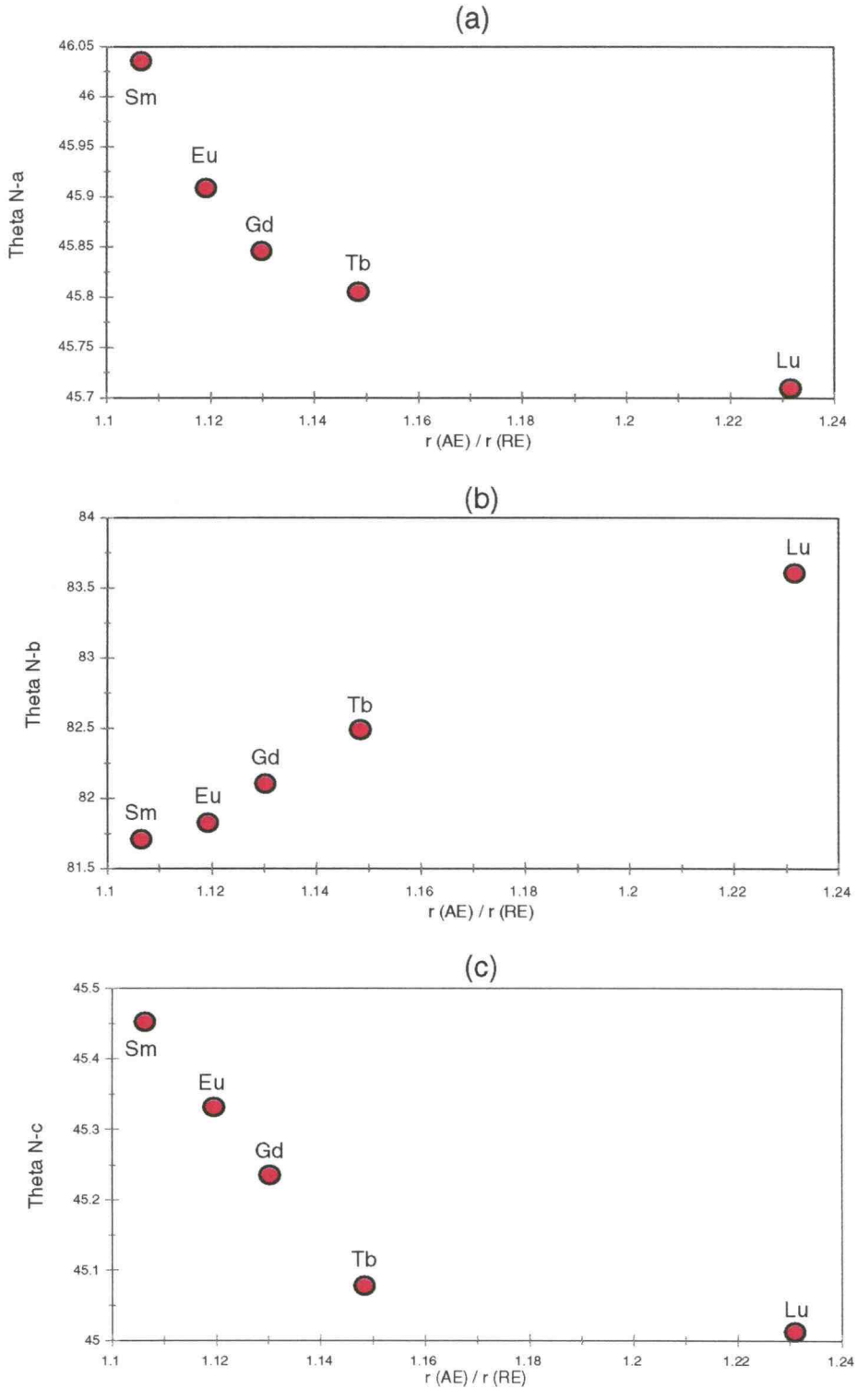

Figure 2.9 Group (I) BO_3 motion relative to the (a) a-axis (b) b-axis and the (c) c-axis.

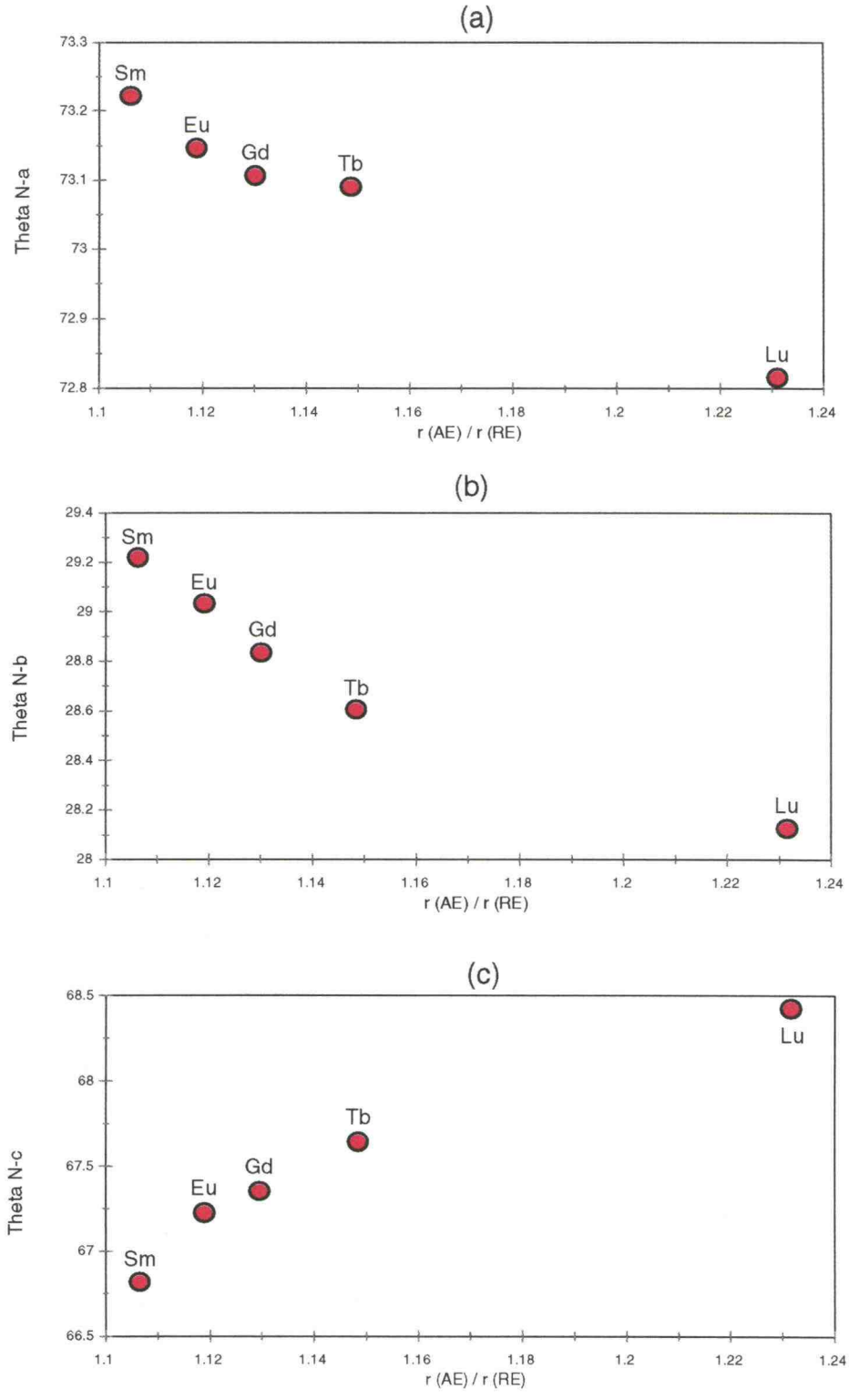

Figure 2.10 Group (II) BO_3 motion relative to the (a) a-axis (b) b-axis and the (c) c-axis.

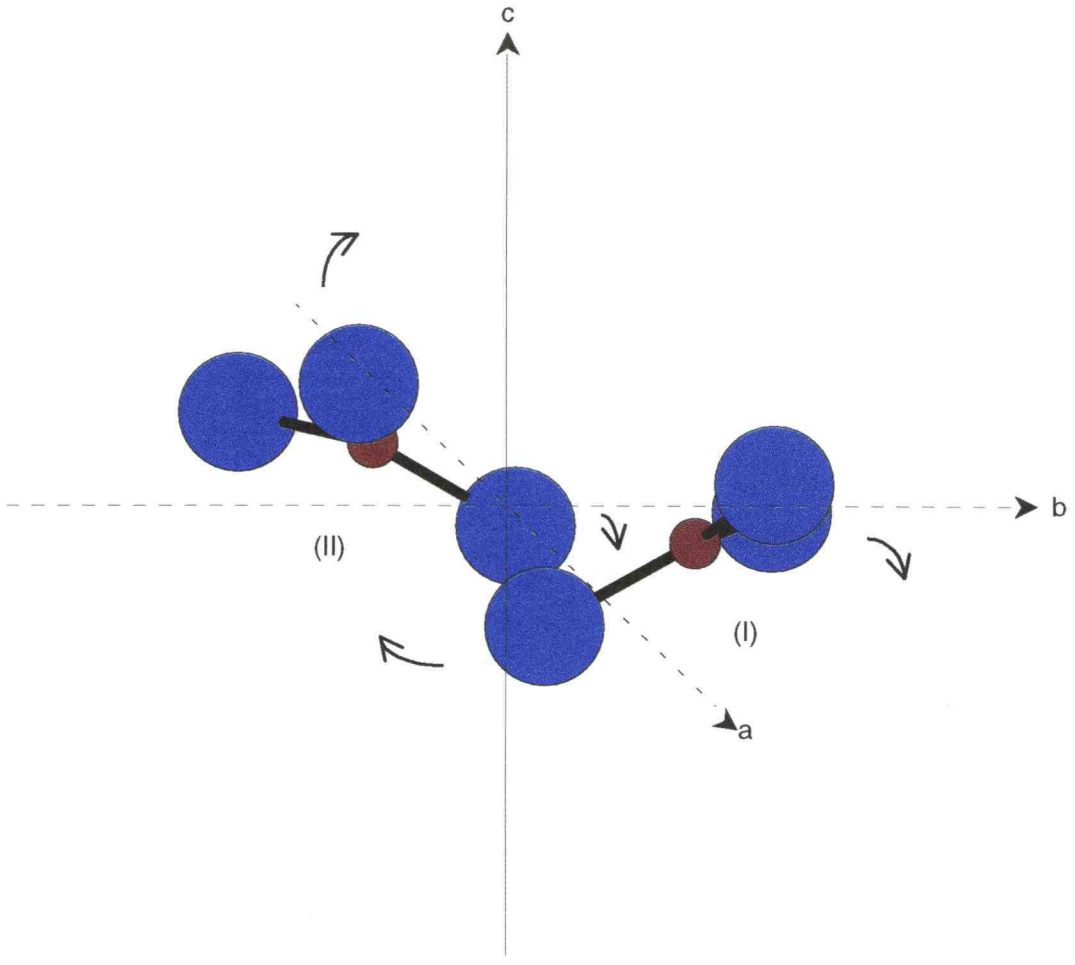

Figure 2.11 Orientation of BO_3 groups (I) and (II) relative to the unit cell axes.

The slopes indicate that in the series Sm>Eu>Gd>Tb>Lu, the group (I) borate is moving away from the *b* axis and into the *ac* plane while the group (II) borates exhibits' movement away from the *c* axis and toward the *ab* plane. Figure 2.11 illustrates this effect by comparing groups (I) and (II) with the unit-cell axes. Since, the remaining B(2) triangles are mirror images, the opposite structural rearrangements apply.

In an alternative interpretation of this data it is suggested that the only significant shifts are away from the *b* and *c* axes for groups (I) and (II) respectively, since, the supplemental data may only reflect some random movement in the structure. As indicated previously, borates exhibit great potential as frequency converters. A program written in this laboratory has been utilized to calculate the second harmonic susceptibility *(d)* coefficients of the lanthanide analogs listed above.

Table 2.12 indicates the matrix of nonzero *d* coefficients for the point group m. Calculated *d* coefficients in units of pm/V for several of the lanthanide

Table 2.12 Susceptibility coefficients for the space group Cm

d_{11}	d_{12}	d_{13}	0	d_{15}	0
0	0	0	d_{24}	0	d_{26}
d_{31}	d_{32}	d_{33}	0	d_{35}	0

analogues are listed in Table 2.13. A plot of the B(2) susceptibility (d_{12}) coefficient (as a percent of the optimum) versus the ratio of the alkaline-earth to lanthanide radii is shown in Figure 2.12. From this plot it is evident that there is a constructive increase in the hyperpolarizibility tensors as borate groups (I) and

Table 2.13 Susceptibility coefficients in units of pm/V for $Ca_4LnO(BO_3)_3$

$Ca_4SmO(BO_3)_3$

0.76	-1.3	0.44	0	0.89	0
0	0	0	-0.89	0	-1.3
0.89	-0.89	0.003	0	0.44	0

$Ca_4EuO(BO_3)_3$

0.82	-1.3	0.44	0	0.95	0
0	0	0	-0.89	0	-1.3
0.95	-0.89	0.003	0	0.44	0

$Ca_4GdO(BO_3)_3$

0.82	-1.3	0.44	0	0.95	0
0	0	0	-0.95	0	-1.3
0.95	-0.95	0.003	0	0.44	0

$Ca_4TbO(BO_3)_3$

0.82	-1.3	0.44	0	0.95	0
0	0	0	-0.95	0	-1.3
0.95	-0.95	0.003	0	0.44	0

$Ca_4LuO(BO_3)_3$

0.95	-1.5	0.44	0	0.95	0
0	0	0	-0.95	0	-1.5
0.95	-0.95	0.003	0	0.44	0

(II) shift away from the *b* and *c* axes. Therefore, the power extracted from a second-harmonic crystal will be a maximum for the smallest lanthanide ion, i.e., Lu, since this will reflect the greatest BO_3 shift. This is further illustrated by Figure 2.13 in which a plot of the volume corrected maximum *d* coefficients against the ratio of the alkaline-earth to lanthanide radii is given. The results suggest that as the radius of the lanthanide ion decreases the susceptibility coefficient increases. Additionally, the BO_3-group reorientation contributes approximately 84% more to the increase of the calculated nonlinear susceptibility than does the increased BO_3-group number density.

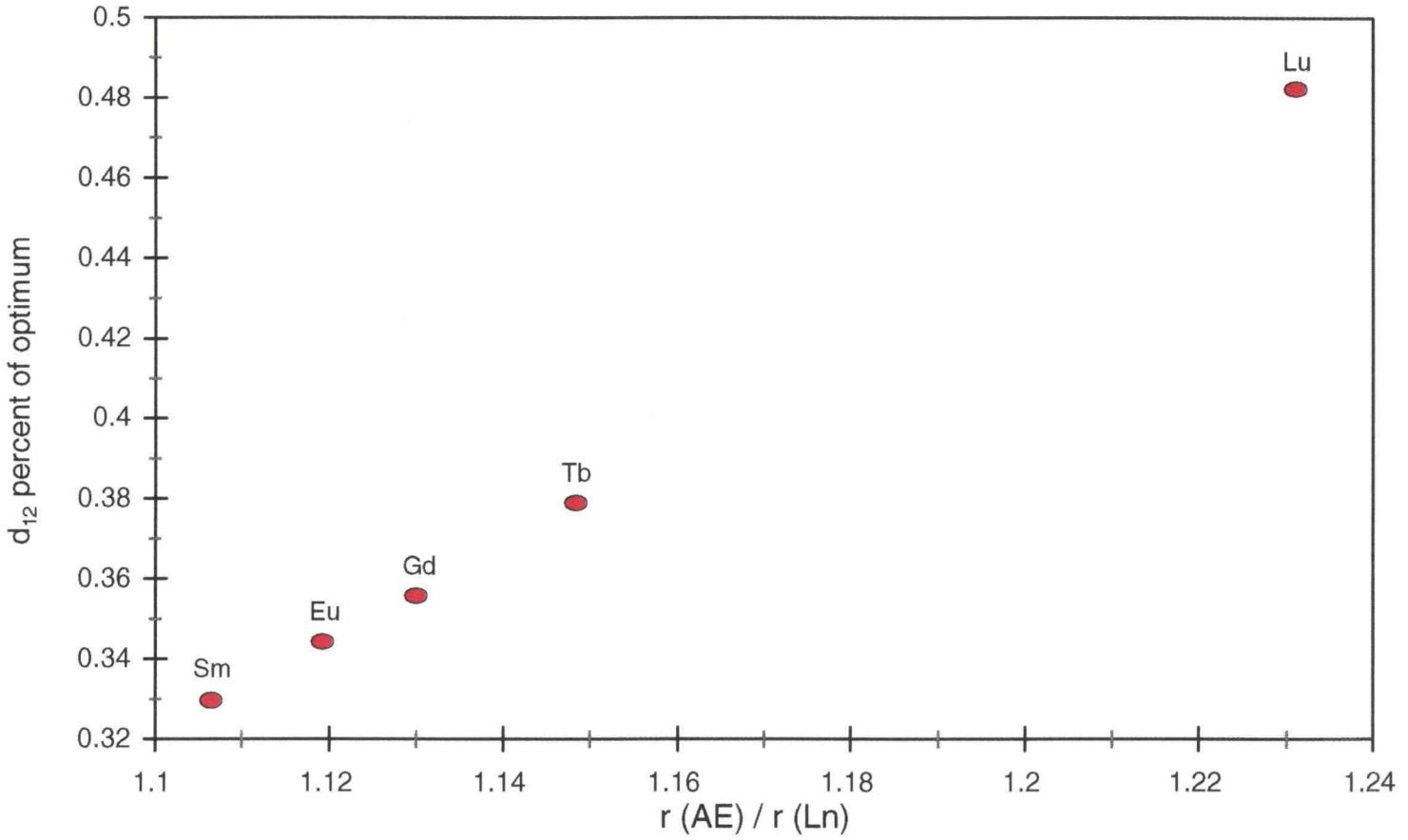

Figure 2.12 B(2) triangle orientation contribution to the calculated d_{12} (percent of optimum) as a function of the ratio of alkaline-earth to lanthanide radii.

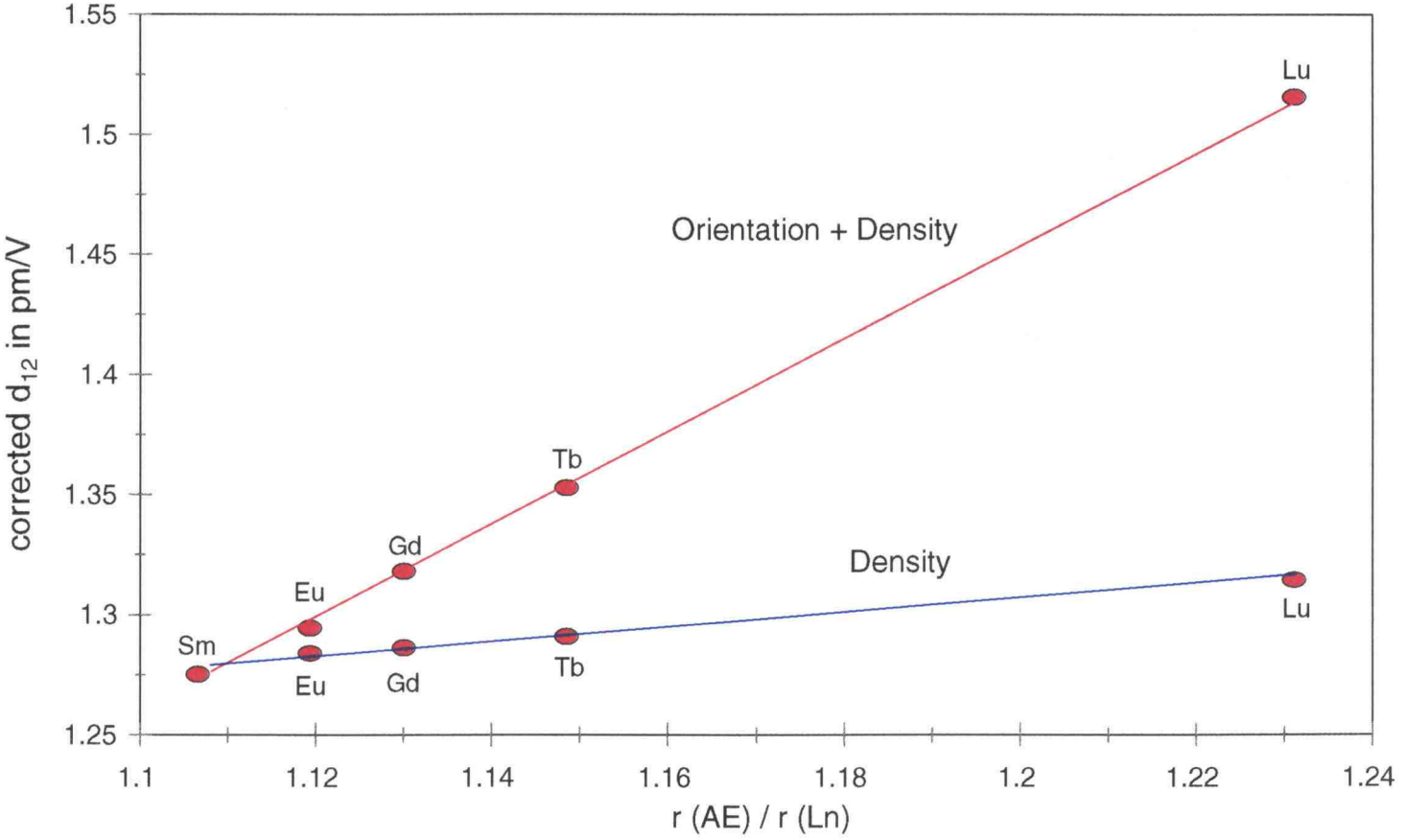

Figure 2.13 Change in the calculated d_{12} in pm/V as a funcition of the ratio of alkaline-earth to lanthanide radii.

Luminescence Study

Figure 2.14 shows the vacuum ultraviolet excitation spectrum of $Ca_{1.76}Sr_{2.24}GdO(BO_3)_3$ and $Ca_{3.38}Mg_{0.62}GdO(BO_3)_3$ relative to sodium salicylate. Two broad bands are observed with peak maxima located near 185 and 240 nm that correspond to host absorption and O-to-Eu charge transfer, respectively. A higher brightness by the Sr substituted analog occurs in both of these regions. The excitation spectrum of $Ca_4YO(BO_3)_3$ shown in Figure 2.15 also exhibits the two bands.

The emission spectrum of Eu^{3+} doped $Ca_4YO(BO_3)_3$ closely resembles that of the common red phosphor Eu^{3+}:Y_2O_3 as seen in Figure 2.16. Chromaticity values for these and related materials are listed in Table 2.14. The chromaticity of Eu^{3+}:$Ca_4YO(BO_3)_3$ is similar to that of Eu^{3+}:Y_2O_3. The occurrence of such striking similarities by two apparently different materials might be unexpected.

Table 2.14 Chromaticity coordinates of borate samples doped with 3% Eu^{3+} and Osram Y_2O_3 standard doped with 5 wt.% Eu^{3+}.

Sample	X	Y
$Ca_4YO(BO_3)_3$	0.647(5)	0.353(5)
$Ca_4LaO(BO_3)_3$	0.649(5)	0.351(5)
$Ca_4GdO(BO_3)_3$	0.649(5)	0.351(5)
$Ca_2Sr_2GdO(BO_3)_3$	0.651(5)	0.349(5)
$Ca_3MgGdO(BO_3)_3$	0.651(5)	0.349(5)
Y_2O_3	0.652(5)	0.348(5)

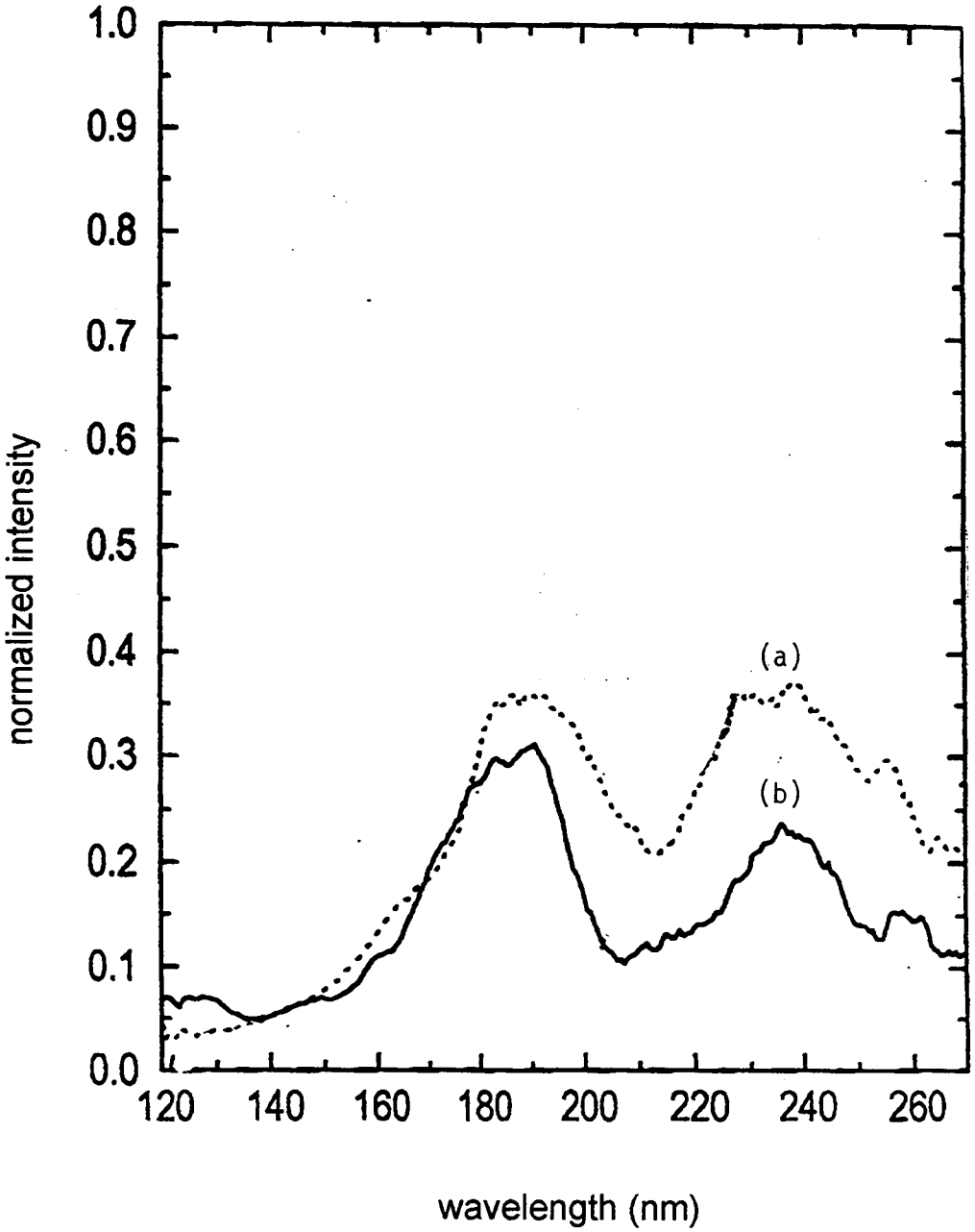

Figure 2.14 Vacuum ultraviolet spectra of 3% Eu^{3+} in (a) $Ca_2Sr_2GdO(BO_3)_3$ and (b) $Ca_3MgGdO(BO_3)_3$

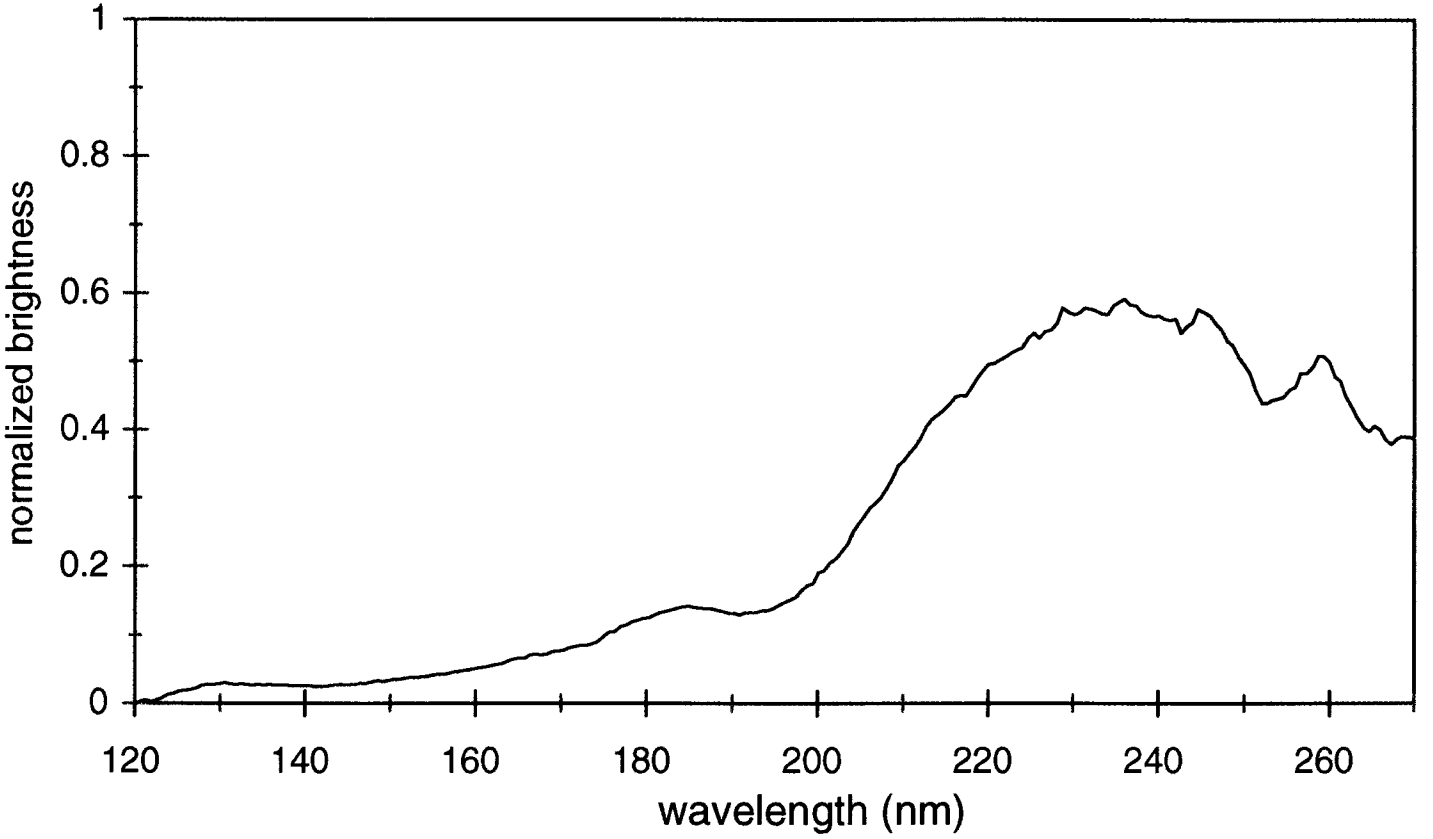

Figure 2.15 Excitation spectrum of 10% Eu^{3+} doped $Ca_4YO(BO_3)_3$, λ_{em}= 612 nm.

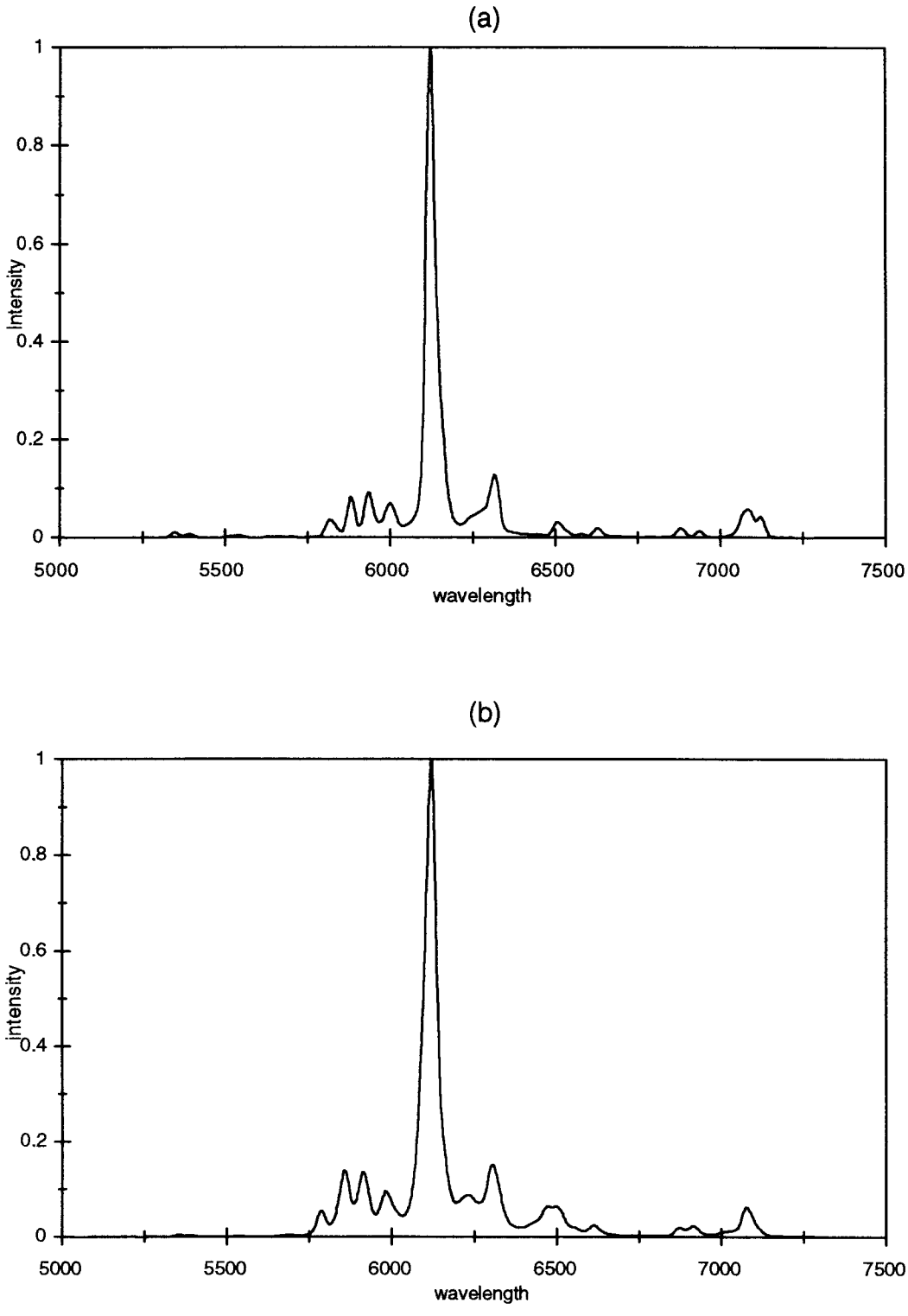

Figure 2.16 Emission spectra of Eu^{3+} doped (a) Y_2O_3 (λ_{exc}= 254 nm) and (b) $Ca_4YO(BO_3)_3$ (λ_{exc}= 254 nm).

To explain these findings, we can more closely examine the lanthanide environment in each material. Drawings of the C_2 and C_s Y sites in Y_2O_3 and $Ca_4YO(BO_3)_3$, respectively, are given in Figure 2.17. The O1-Y-O2 bond angles differ by less than 7° between the two octahedra. The O3-Y-O4 and O5-Y-O6 bond angles differ by approximately 5°. These angles are seemingly one prerequisite to obtaining the saturated red emission. By evaluating the distortions at the luminescent center one may anticipate emission "fingerprints" such as these in other materials.

Figure 2.18 depicts the brightness of Eu^{3+}:$Ca_4YO(BO_3)_3$ relative to that of Eu^{3+}:Y_2O_3 as a function of Eu^{3+} concentration. Although, the brightness increases through the addition of 10 mol% Eu^{3+}, the observed intensity does not augment correspondingly with the increased concentration of dopant ions. This is typical of concentration quenching at higher Eu^{3+} dopant levels. As previously stated, the lanthanide ions connect via shared octahedra to form linear chains along the *c* axis. With an increasing concentration of Eu^{3+} ions the probability for these ions to become located adjacent to one another increases. Energy transfer between such ions would mediate the possibility of thermal deactivation with structural defects. However, Y_2O_3 is much less affected in this manner. In Y_2O_3 the luminescent center is isolated from other metal sites. Excited europium ions are therefore left with only two routes back to the ground state, since, the ion is unable to transfer its energy to another luminescent site. These routes are of course the emission of photons or thermal decay.

Brightness studies show that the intensity of $Ca_4YO(BO_3)_3$ doped with 10 mol% Eu^{3+} (4.46×10^{20} Eu atoms/cm^3) is found to be 55% of the intensity obtained

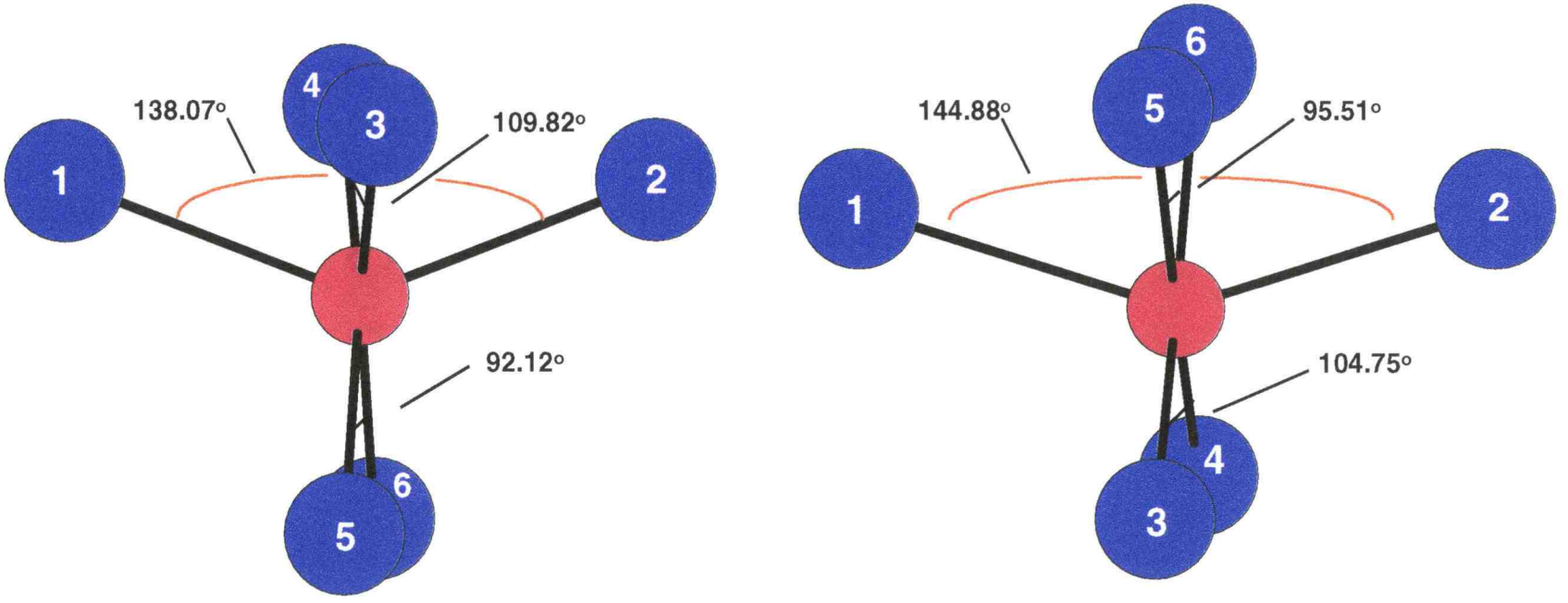

(a) (b)

Figure 2.17 Drawing of the octahedra around the C_2 yttrium site in (a) Y_2O_3 and the C_s yttrium site in (b) $Ca_4YO(BO_3)_3$.

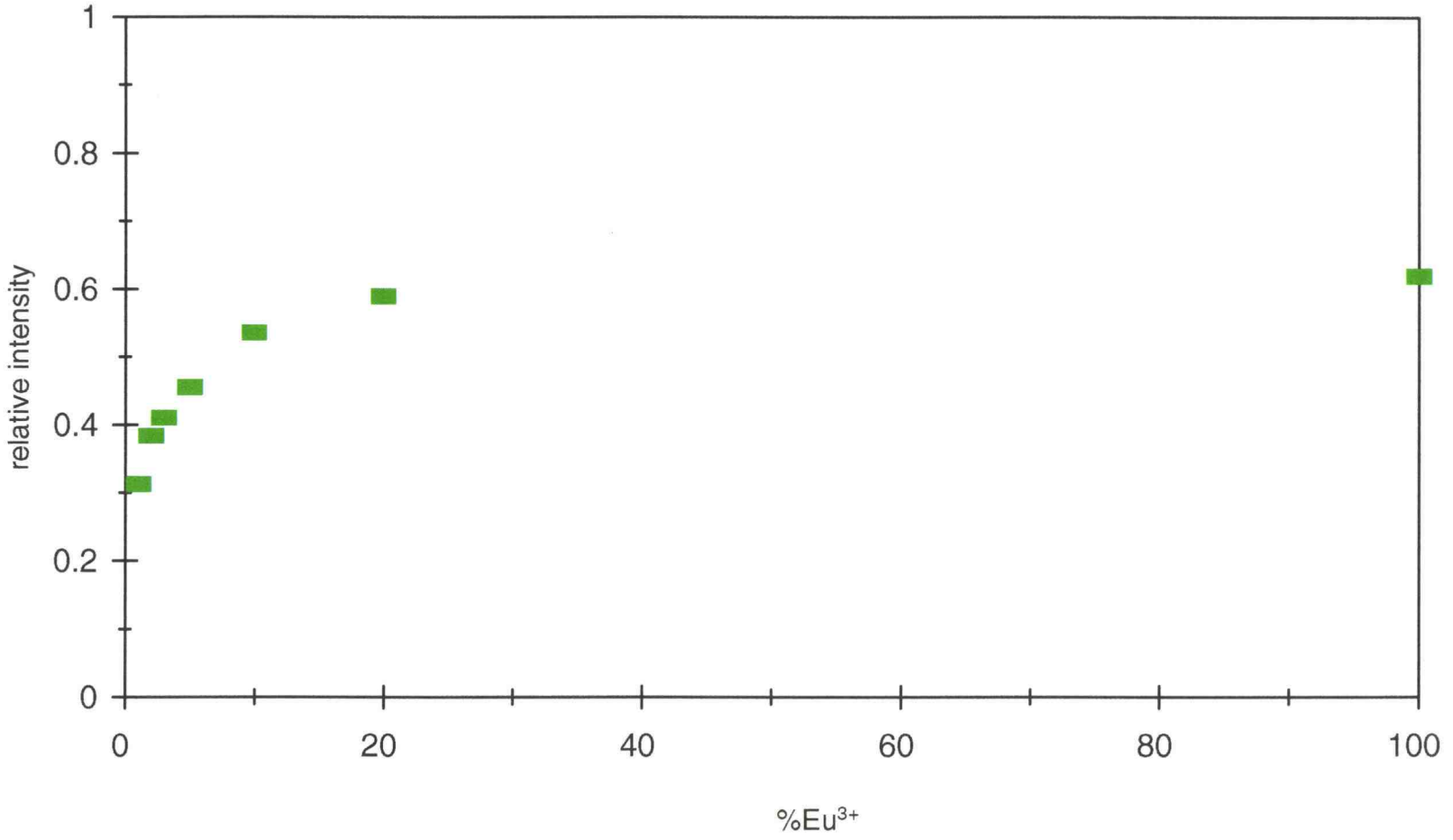

Figure 2.18 Eu^{3+} concentration study of the $Ca_4YO(BO_3)_3$ brightness relative to Y_2O_3.

from the Y_2O_3 standard. However, commercial Y_2O_3 doped with 3.5 mole% Eu^{3+} ($8.58x10^{20}$ Eu atoms/cm^3) also contains 52% more ions, all of which may be utilized in photon emission. Although, the maximum intensity observed from the borate correlates with its number of luminescent centers, it is impossible for the borate material to effectively harness an increased number density of Eu^{3+} in the chained network since this increases concentration quenching events.

The curve in Figure 2.19 represents the thermal quenching of Eu^{3+}:$Ca_4YO(BO_3)_3$. Only slight quenching occurs from 4.2 to 525 K where the lifetime decreases by 0.01 ms. We conclude that the quantum efficiency is relatively high and likely approaches that of Eu^{3+}:Y_2O_3. In Figure 2.20, the analogues Ca_4(Y, La, Gd)$O(BO_3)_3$ exhibit a decrease by 15% from their initial intensities over the temperature range 298-525 K.

Brightness, as expected, strongly increases with higher preparative temperature. Figure 2.21 shows the normalized relative intensity of $Ca_4YO(BO_3)_3$ doped with 10% Eu^{3+} at 900 and 1100 °C over various reaction times. Within the first 3-4 hours of heating at 900 °C, the sample brightness increases to 60% of the observed maximum. Continuation at this temperature leads to only a 6-7% increase. The brightness reaches a maximum within 4 hours after the temperature is increased to 1100 °C. The sample shows approximately 98% of the maximum intensity after firing for only 5 hours.

The Eu^{3+} doped $Ca_4YO(BO_3)_3$ powder particles were determined to be in the range of 1-10 microns as determined by scanning electron microscopy (Figure 2.22).

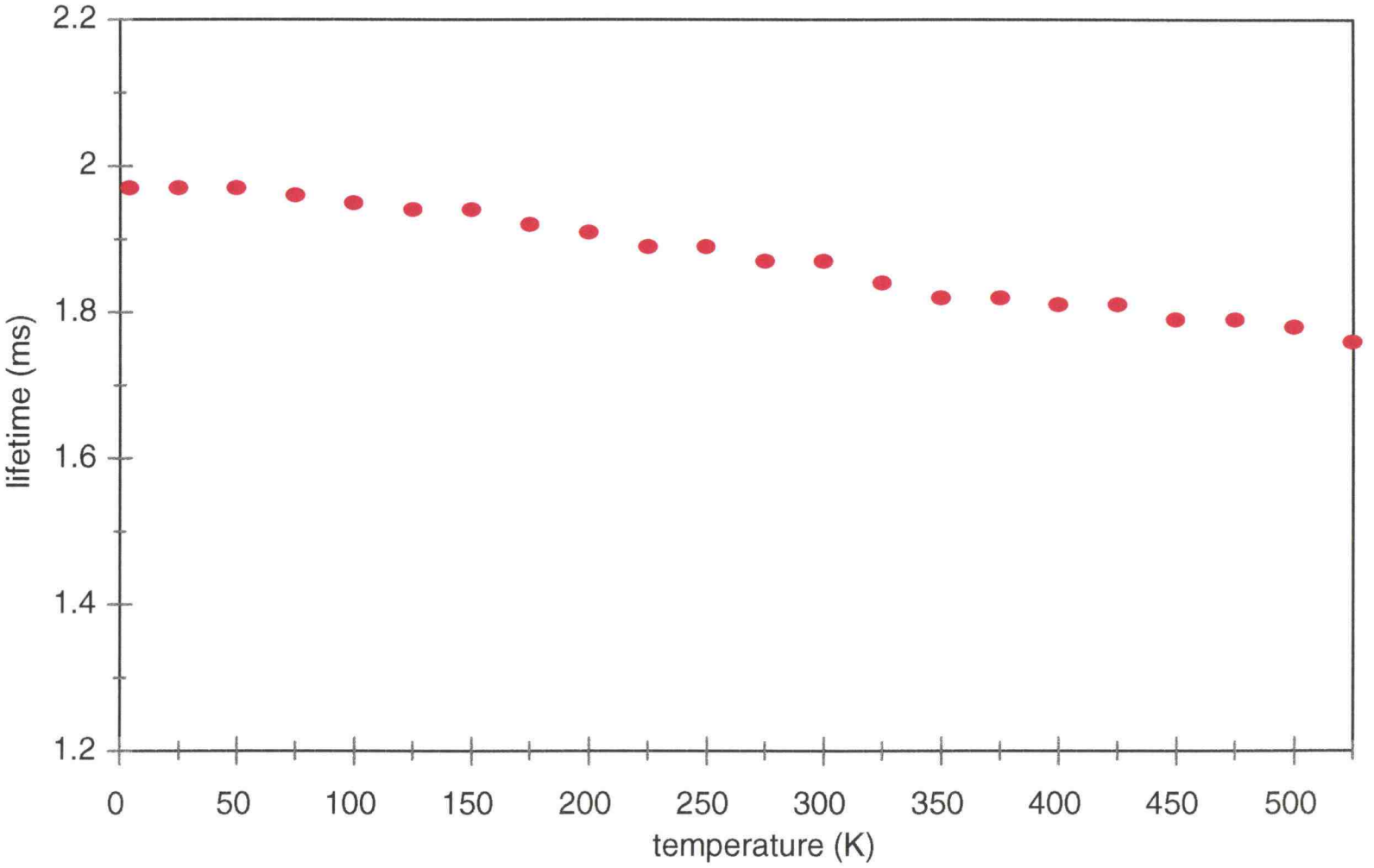

Figure 2.19 Thermal quenching of Eu^{3+} doped $Ca_4YO(BO_3)_3$.

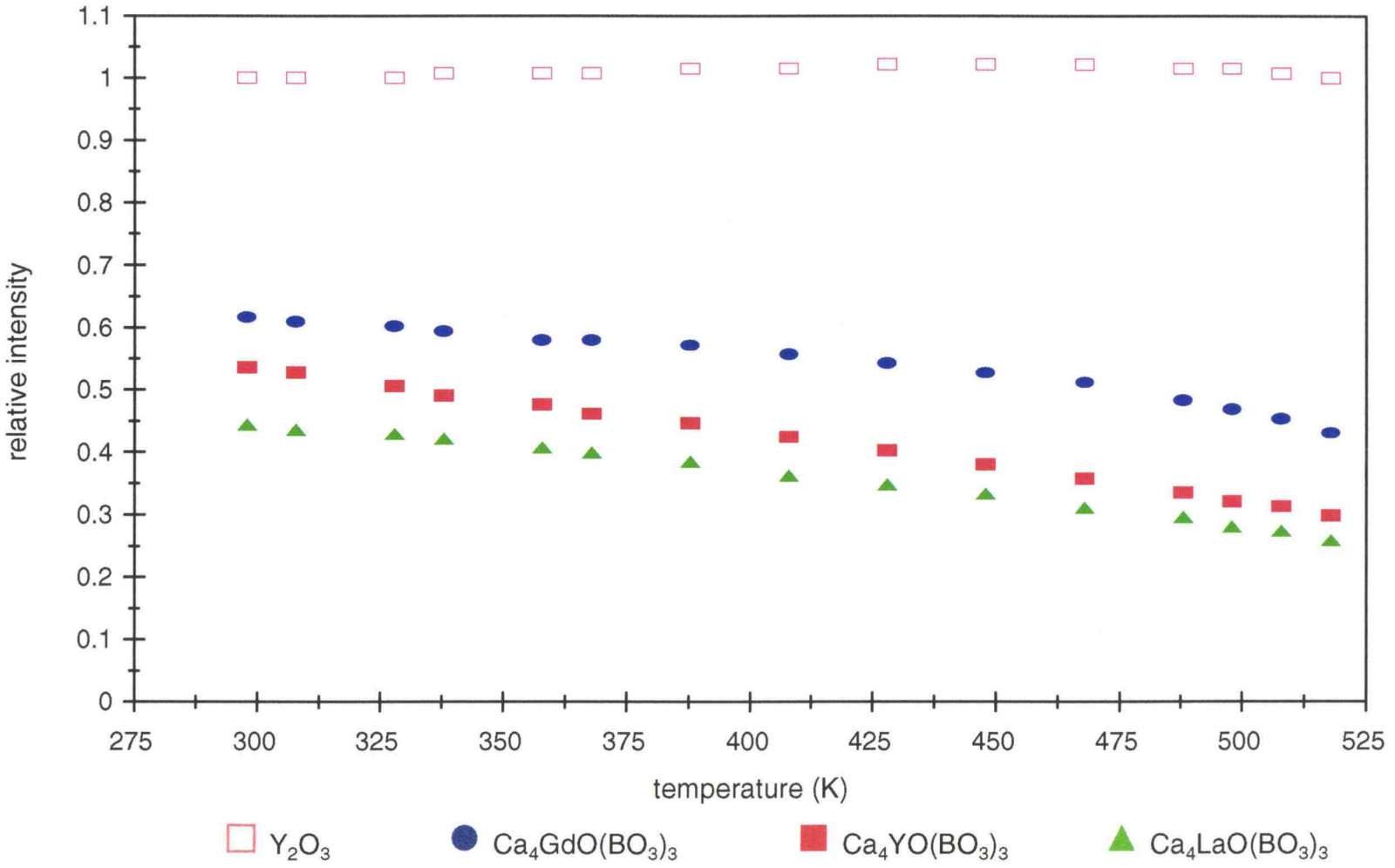

Figure 2.20 Temperature dependent brightness of Eu^{3+} doped $Ca_4(Gd,Y,La)O(BO_3)_3$ relative to Y_2O_3.

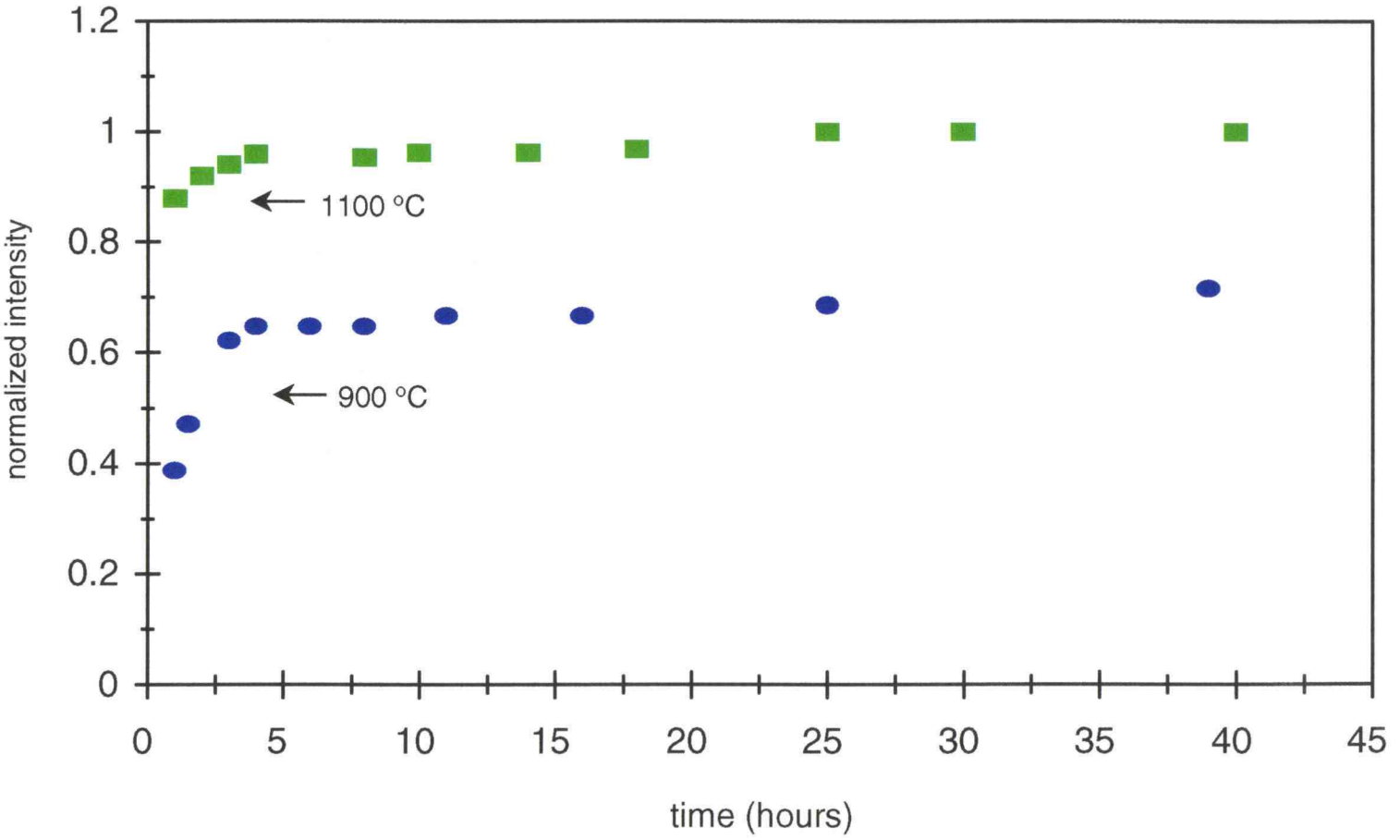

Figure 2.21 Brightness of Eu^{3+} doped $Ca_4YO(BO_3)_3$ relative to firing duration and temperature.

(a)

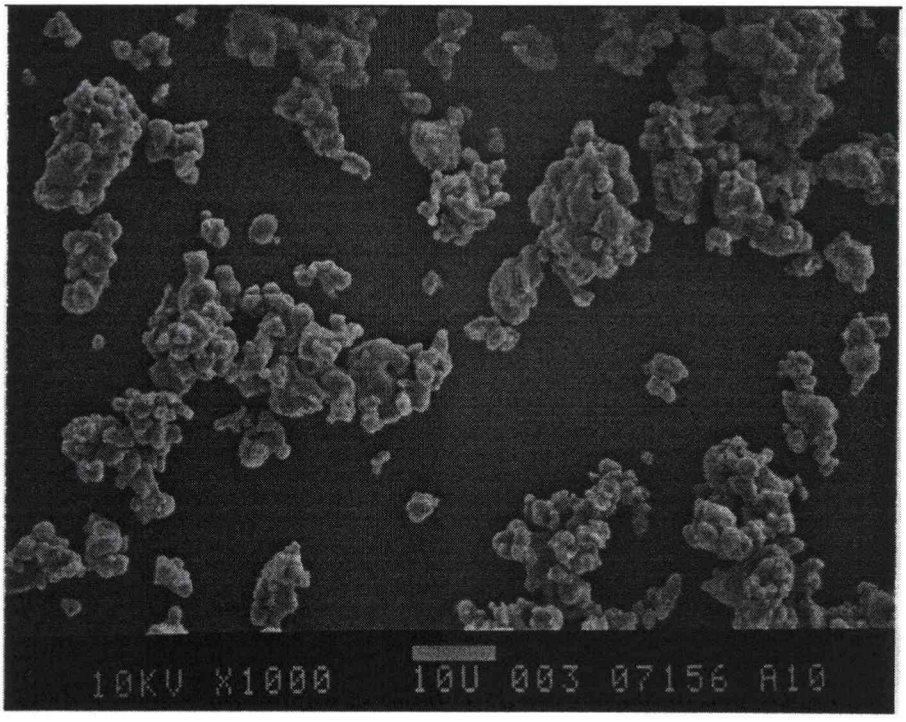

(b)

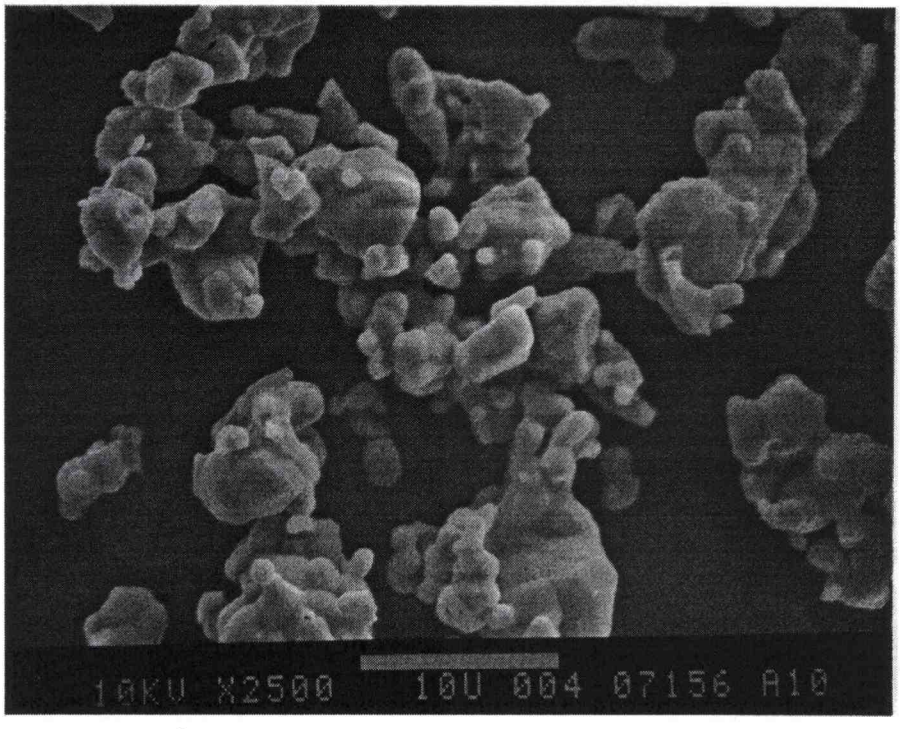

Figure 2.22 Scanning electron micrographs of Eu^{3+} doped $Ca_4YO(BO_3)_3$ at (a) 1000x and (b) 2500x resolution.

Conclusions:

Structural evaluation of the tetracalcium lanthanide borate oxide family of materials, such as alignment of the borate groups, and the geometry around the lanthanide ion, have provided both fundamental and practical insight into the properties of these materials.

By identifying materials with luminescent centers that parallel those found in both the $Ca_4LnO(BO_3)_3$ and Y_2O_3, one may predict the likelihood of favorable properties of red emitting phosphors. Also, it seems particularly relevant that the luminescent centers in a prospective phosphor are isolated from equivalent metal sites in order to minimize energy losses. Luminescent studies indicate that the analog $Ca_4YO(BO_3)_3$ is both chromatically viable and efficient with respect to its Eu^{3+} emission. Additionally, this material might afford certain economic advantages over the industry standard Eu^{3+}:Y_2O_3. However, in spite of these desirable features it seems unlikely that the brightness of Y_2O_3 can be approached more closely than within 50-70% of Eu^{3+}:Y_2O_3 because of concentration quenching at higher dopant levels.

The optical characteristics for this class of metal borate oxide indicate promising results for second harmonic frequency conversion applications. It has been demonstrated that for maximum power conversion through such a crystal, the size of the atom occupying the rare earth site should be minimized. Since, these materials melt congruently it should be possible to grow large, optically clear crystals.

References:

1. G. Blasse, B. C. Grabmaier, *Luminescent Materials*, Chapter 3, New York: Springer-Verlag, 1994.

2. K. Sudarsanan, P. E. Mackie, R. A. Young, *Mater. Res. Bull.* **7**, 1331, (1972).

3. R. Norrestam, M. Nygren, *Chem Mater.* **4**, 737, (1992).

4. G. J. Dirksen, G. Blasse, *J. All. Comp.* **191**, 121, (1993).

5. B. R. Judd, *Phys. Rev.*, **127**, 750, (1966).

6. G. S. Ofelt, *J. Chem. Phys.*, **37**, 511, (1966).

7. C. Chen *et al.*, *J. Opt. Soc. Am.*, **B6**, 616, (1989).

8. Molecular Structure Corporation, TEXSAN, Single Crystal Structure Analysis Software, Version 5.0 (1980). MSC 3200 A Research Forest Drive, The Woodlands, TX 77381, USA.

9. G. M. Sheldrick, "Crystallographic Computing 3, "Eds. G. M. Sheldrick, C. Krüger, and R. Goddard, pp. 175-189, Oxford University Press, Oxford (1985).

10. N. Walker and D. Stuart, *Acta Crystallogr.*, Sect. A **39**, 158, (1983).

11. Dowty, E. ATOMS. A computer program for displaying atomic structures, Kingsport, (1989).

12. A. B. Ilyuknin, B. F. Dzhurinskii, *Zhumal NeoOrganicheskoi Khimii*, 38, 917, (1993).

BIBILIOGRAPHY

1. M. J. Weber, *CRC Handbook of Laser Science and Technology*, "Section 1: Nonlinear Optical Materials", Boca Raton, Fla.: CRC Press, 1986.

2. G. Blasse, A. Bril, W. C. Nieuwpoort, *J. Phys. Chem. Solids.*, **27**, 1587-1592, (1966).

3. G. Blasse, *J. Solid State Chem.*, **4**, 52-54, (1972).

4. B. Saubat, C. Fouassier, P. Hagenmuller, *Mat. Res. Bull.*, **16**, 193-198, (1981).

5. G. A. West, N. S. Clements, *J. Luminescence*, **54**, 245-248, (1992).

6. B. R. Judd, *Phys. Rev.*, **127**, 750, (1966).

7. G. S. Ofelt, *J. Chem. Phys.*, **37**, 511, (1962).

8. G. Blasse, B. C. Grabmaier, *Luminescent Materials*, Chapter 3, New York: Springer-Verlag, 1994.

9. K. Sudarsanan, P. E. Mackie, R. A. Young, *Mater. Res. Bull.* **7**, 1331, (1972).

10. R. Norrestam, M. Nygren, *Chem Mater.* **4**, 737, (1992).

11. G. J. Dirksen, G. Blasse, *J. All. Comp.* **191**, 121, (1993).

12. B. R. Judd, *Phys. Rev.*, **127**, 750, (1966).

13. G. S. Ofelt, *J. Chem. Phys.*, **37**, 511, (1966).

14. C. Chen *et al.*, *J. Opt. Soc. Am.*, **B6**, 616, (1989).

15. Molecular Structure Corporation, TEXSAN, Single Crystal Structure Analysis Software, Version 5.0 (1980). MSC 3200 A Research Forest Drive, The Woodlands, TX 77381, USA.

16. G. M. Sheldrick, "Crystallographic Computing 3, "Eds. G. M. Sheldrick, C. Krüger, and R. Goddard, pp. 175-189, Oxford University Press, Oxford (1985).

17. N. Walker and D. Stuart, *Acta Crystallogr.*, Sect. A **39**, 158, (1983).

18. Dowty, E. ATOMS. A computer program for displaying atomic structures, Kingsport, (1989).

19. A. B. Ilyuknin, B. F. Dzhurinskii, *Zhurnal NeoOrganicheskoi Khimii*, 38, 917, (1993).

20. T. Welker, *J. of Luminescence*, **48-49**, 49-56, (1991).

21. A. W. Veenis, A. Bril, *Philips J. Res.*, **33**, 124-132, (1978).

22. G. Blasse, *J. Chem. Phys.*, **45**, 2356, (1966).

23. G. Blasse, A. Bril, W. C. Nieuwpoort, *J. Phys. Chem. Solids*, **27**, 1587-1592, (1966).

24. J. D. Dunitz, *X-Ray Analysis and the Structure of Organic Molecules*, Cornell University Press, 495, (1979).

APPENDICES

APPENDIX 1

Luminescence of Eu^{3+} In Selected Hosts

Luminescent materials can be defined as those substances that, upon excitation, emit light through some energy-conversion process. Phosphors are those luminescent materials that find application in areas such as fluorescent lighting, color television, and plasma displays. It is important that these phosphors exhibit high brightness, generally by minimizing nonradiative energy losses. In this way, conversion of the absorbed energy to emitted light can be maximized. Phosphors used in these devices must also endure long durations of exposure to UV, VUV, and electron influences. Currently, the red emitting phosphors used in the three devices listed above, are Eu^{3+} doped Y_2O_3, Y_2O_2S, and $Y_{0.75}Gd_{0.25}BO_3$, respectively. However, the expense of yttrium oxide (1) and the poor chromaticity of the lanthanide borate (2) provide impetus for the search for alternative materials.

One method of searching for new materials entails preparing a large selection of different phosphor candidates. Samples are then evaluated on the basis of specific, measurable, luminescent properties. By comparing and contrasting these properties over a vast number of samples, it may be possible to identify trends that relate structural and luminescent characteristics. Two properties routinely evaluated include (i) brightness relative to a standard material (ii) and the observed chromaticity.

The phosphor's brightness depends both on its emission efficiency and

the ability to absorb the source excitation energy. For strongly absorbing materials, highly intense emissions may be obtained. Once absorbed, the energy undergoes a conversion process that ends with radiative or nonradiative decay from the host material. For example, materials with high quantum efficiencies can deactivate effectively through radiative processes. This is true of materials with charge transfer onsets located at higher energies (3). For *red* emitting phosphors that utilize Eu^{3+} as the activator ion, it is of some importance for the host material to possess a dopant site that deviates from inversion symmetry. This allows the *red* $^5D_0 \rightarrow {}^7F_2$ transition to dominate over the *orange* $^5D_0 \rightarrow {}^7F_1$ line (4).

In this study powdered samples of several materials were prepared by high temperature solid-state methods. Stoichiometric quantities of high purity oxides, nitrates, and carbonates were mixed and decomposed at 800 °C for 1 h followed by grinding and heating at appropriate temperatures overnight with intermittent grinding. The resulting powders were confirmed to be single phase and the correct structure by comparing experimental X-ray diffraction patterns to calculated patterns. Spectral data were obtained by using the methods previously described. Chromaticity values were calculated by using software written in this laboratory. Data are summerized in Table A1.1.

A Eu^{3+}:$Gd_2MoB_2O_9$ excitation spectrum extending into the VUV is shown in Figure A1.1a. Two broad absorption bands with maxima at 176 and 230 nm are easily identified. These correspond to the host and O-to-Eu charge transfer, respectively. The emission spectrum in Figure A1.1b features an intense $^5D_0$

Table A1.1 List of materials analyzed for brightness relative to Eu:Y_2O_3, position of the charge transfer band, and chromaticity values.

Compound	I (Y2O3)	X	Y
Eu:Y_2O_3	1	0.652(5)	0.348(5)
Eu(10%):$LaBSiO_5$	0.2679	0.645(5)	0.355(5)
Eu(10%):$LaBGeO_5$	0.1429	0.641(5)	0.359(5)
Eu(10%):$LaB(SiO_4)_{0.5}(GeO_4)_{0.5}O$	0.2232	0.638(5)	0.362(5)
Eu(10%):$GdBGeO_6$	0.4821	0.640(5)	0.360(5)
Eu(10%):$LaBWO_6$	0.0538	0.662(5)	0.337(5)
Eu(10%):$Gd_2MoB_2O_9$	0.1429	0.649(5)	0.351(5)
Eu(5%):$Ca_2B_2P_2O_{10}$	0.2317	0.619(5)	0.381(5)
Eu(5%):$Ba_2B_2P_2O_{10}$	0.2195	0.615(5)	0.384(5)
Eu(3%):$GdBO_3$	0.2973	0.642(5)	0.358(5)
Eu(3%):$LaBO_3$	0.2589	0.651(5)	0.349(5)
Eu(5%):$La_4B_2WO_{12}$	0.0268	0.664(5)	0.335(5)
Eu(3%):$Ca_4LaO(BO_3)_3$	0.4001	0.649(5)	0.351(5)
Eu(3%):$Ca_4GdO(BO_3)3$	0.4595	0.649(5)	0.352(5)
Eu(3%):$Ca_4YO(BO_3)_3$	0.4144	0.647(5)	0.353(5)
Eu(3%):$Ca_3MgGdO(BO_3)_3$	0.2321	0.651(5)	0.349(5)
Eu(3%):$Ca_2Sr_2GdO(BO_3)_3$	0.3125	0.651(5)	0.349(5)
$Eu_4B_2WO_{12}$	0.0446	0.657(5)	0.342(5)

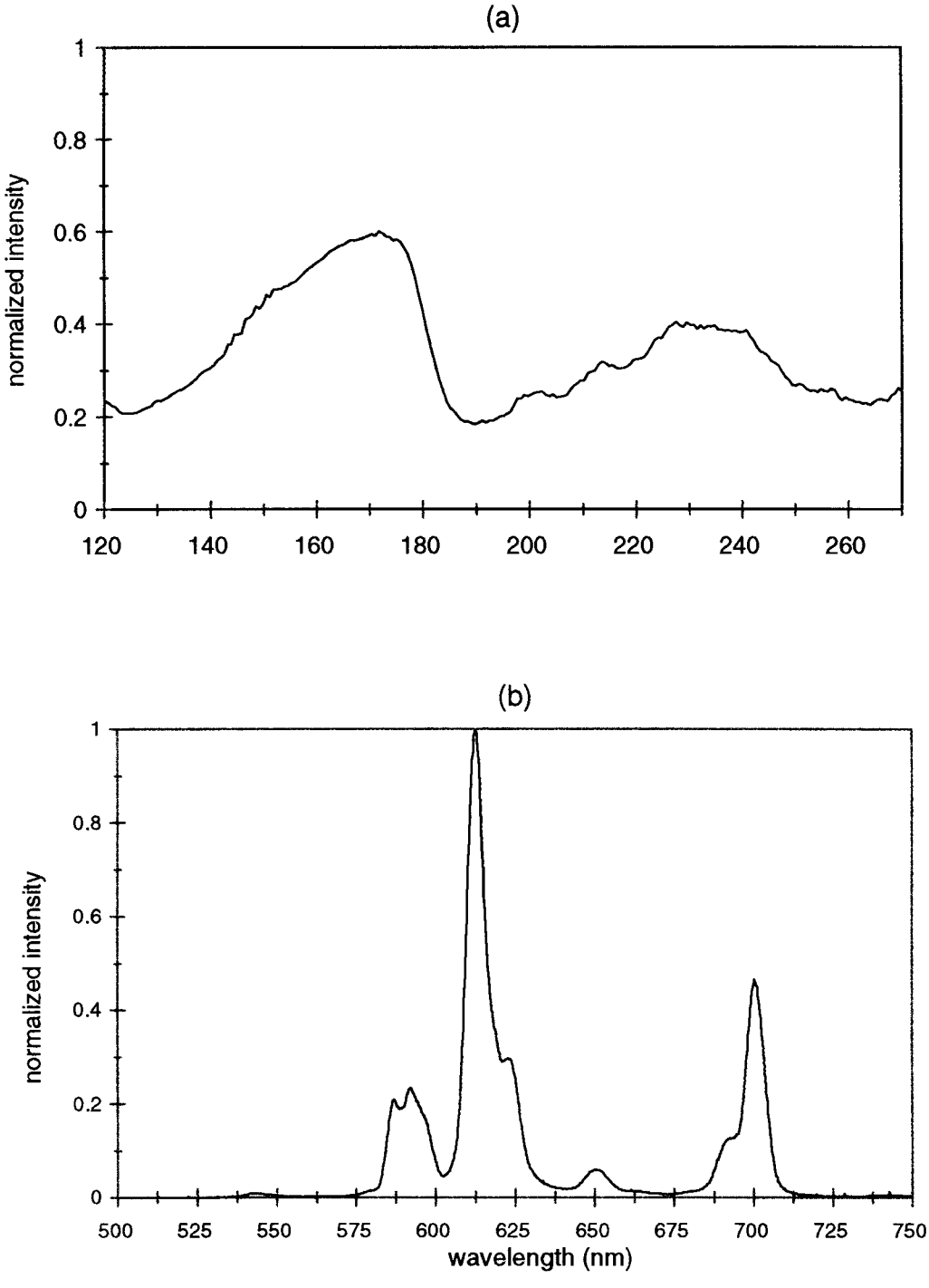

Figure A1.1 The (a) excitation of Eu^{3+} doped $Gd_2MoB_2O_9$ (λ_{em}= 612 nm) in the vacuum uv and (b) the emission spectrum (λ_{exc}= 254 nm).

$\rightarrow {}^7F_2$ transition. Those wavelengths for several materials that produce brightness maxima are listed in Table A1.2; all data are scaled to sodium salicylate.

Table A1.2 Brightness relative to sodium salicylate. Vacuum ultraviolet measurements were performed at the University of Georgia.

Compound	absorption wavelengths		
	147 nm	185 nm	254 nm
Eu(3.5%):Y_2O_3 (Osram)	0.80	1.68	1.38
Eu(10%):$LaBMoO_6$	<0.05	<0.05	<0.05
Eu(10%):$Gd_2MoB_2O_9$	0.42	0.20	0.30
Eu(3%):$GdBO_3$	0.60	0.15	0.25
Eu(20%):$La_4B_2WO_{12}$	0.05	<0.05	0.10
Eu(10%):$Ca_4GdO(BO_3)_3$	0.10	0.50	0.72
Eu(3%):$Ca_4YO(BO_3)_3$	0.05	0.15	0.50
$Ca_4EuO(BO_3)_3$	0.10	0.45	0.75

From the data, it appears that the host $Gd_2MoB_2O_9$ should be examined in more detail. The emission brightness is approximately 70% of that of $GdBO_3$, so a study of the effects of the substitution $Gd_{2-x}Y_xMoB_2O_9$ should be undertaken. The high intensity of the ${}^5D_0$-${}^7F_4$ transition near 700-nm may be an unacceptable loss, but this intensity should be monitored as a function of Y substitution. The decreased intensity in the ${}^5D_0$-${}^7F_1$ transition relative to that of Eu^{3+}:$Y_{0.75}Gd_{0.25}BO_3$ also provides an improved chromaticity.

References:

1. T. Welker, *J. of Luminescence*, **48-49**, 49-56, (1991).

2. A. W. Veenis, A. Bril, *Philips J. Res.*, **33**, 124-132, (1978).

3. G. Blasse, *J. Chem. Phys.*, **45**, 2356, (1966).

4. G. Blasse, A. Bril, W. C. Nieuwpoort, *J. Phys. Chem. Solids*, **27**, 1587-1592 (1966).

APPENDIX 2

BO_3 Orientation Program

The following program was written to determine the reorientation that borate triangles undergo within the unit cells of the $Ca_4LnO(BO_3)_3$ analogs (Ln = lanthanide atoms). The user must first input the unit cell parameters of the crystal which are then converted into parameters associated with the cartesian system. The code for this conversion was taken from Dunitz (1). The user then enters the positions of three atoms in order to define a plane with the cell. Next, the normal vector to this plane is determined from the cross product of two vectors that define that plane. The angles between the normal vector and the cartesian axes are found from the dot product of the normal and the axes. These angles are the program output.

```
90 REM ** CRYSTAL DATA INPUT **
100 CLS
110 DIM x(10), y(10), z(10)
120 REM ** CELL PARAMETERS **
130 PRINT "a,b,c,alpha,beta,gamma"
140 INPUT a1, a2, a3, w1, w2, w3
150 PRINT

160 REM ** CRYSTAL TO CARTESIAN CONVERSION **
170 p = 3.14159 / 180: q = 180 / 3.14159
180 c1 = COS(w1 * p)
190 c2 = COS(w2 * p)
200 c3 = COS(w3 * p)
210 s3 = SIN(w3 * p)
220 m6 = (c1 - c3 * c2) / s3
230 v = SQR(1 - c1 * c1 - c2 * c2 - c3 * c3 + 2 * c1 * c2 * c3)
240 m9 = v / s3
```

```
250 REM ** ATOM POSITIONS **
260 FOR L = 1 TO 3
270 PRINT "What is the oxygen"; L; "position (x,y,z)";
280 INPUT x(L), y(L), z(L)
290 u = a1 * x(L) + a2 * y(L) * c3 + a3 * z(L) * c2
300 v = a2 * y(L) * s3 + a3 * z(L) * m6
310 w = a3 * z(L) * m9
320 x(L) = u
330 y(L) = v
340 z(L) = w
380 NEXT L


390 REM ** PLANE VECTORS PQ AND QR **
400 dX21 = x(2) - x(1)
410 dY21 = y(2) - y(1)
420 dZ21 = z(2) - z(1)
430 dX32 = x(3) - x(2)
440 dY32 = y(3) - y(2)
450 dZ32 = z(3) - z(2)
460 PRINT


490 REM ** NORMAL VECTOR (N) = PQ x QR **
500 i = dY21 * dZ32 - (dY32 * dZ21)
510 j = dX21 * dZ32 - (dX32 * dZ21)
520 k = dX21 * dY32 - (dX32 * dY21)


525 REM ** CALCULATE ANGLES **
530 j = -j
560 N = SQR(i * i + j * j + k * k)
580 i = SQR(i * i): k = SQR(k * k): j = SQR(j * j)
590 IF i < .0000001 THEN i = 0
600 IF j < .0000001 THEN j = 0
610 IF k < .0000001 THEN k = 0
630 IF i = 0 THEN GOTO 640 ELSE GOTO 660
640 ThetaNa = 90
650 GOTO 670
660 ThetaNa = ATN((SQR(N * N - i * i) / i))
670 IF j = 0 THEN GOTO 680 ELSE GOTO 700
680 ThetaNb = 90
690 GOTO 710
700 ThetaNb = ATN((SQR(N * N - j * j) / j))
710 IF k = 0 THEN GOTO 720 ELSE GOTO 740
720 ThetaNc = 90
```

```
730 GOTO 750
740 ThetaNc = ATN((SQR(N * N - k * k) / k))


745 REM ** OUTPUT THE RESULTS **
750 PRINT "The angles between the normal and the cartesian axes are:"
760 PRINT
770 PRINT "a"; ThetaNa * q
780 PRINT "b"; ThetaNb * q
790 PRINT "c"; ThetaNc * q
800 PRINT
810 PRINT "Do you want to calculate another set of angles (y or n)";
820 INPUT try$
830 IF try$ = "y" THEN GOTO 840 ELSE 860
840 PRINT
850 GOTO 110
860 END
```

References:

1. J. D. Dunitz, *X-Ray Analysis and the Structure of Organic Molecules*, Cornell University Press, 495, (1979).

APPENDIX 3

Stoichiometry Program

The following program is designed to calculate the mass of reagents required to synthesize a desired mass of product. The user must input data that includes the empirical formula of the starting reagents and product, the balanced coefficients, and the mass of the product that is to be synthesized. The motivation for this program stems from the repetition involved in performing solid state reactions. This program is very useful and significantly decreases the time required to perform simple stoichiometric calculations. There are, however, several weaknesses inherent to this code. First, the code is "unfriendly" to the user and does not handle mistakes made during data input. Next, the formulas entered by the user must be empirical (i.e., no parentheses). Finally, the program only anticipates a yield of one product for the reaction. Although, this is generally true for solid state reactions, it is untrue for other reaction types.

```
90 REM ** DIMENSION ARRAYS **
100 CLS
110 CLEAR
120 DIM element$(103): DIM e$(100)
130 DIM atoms$(100): DIM cc$(100)
140 DIM mmass(103): DIM em(100)
150 DIM cmp$(100): DIM mascmp(100)
160 DIM moles(100)

200 REM ** READ ELEMENTS AND ATOMIC MASSES **
210 n = 1
220 READ element$(n)
230 READ mmass(n)
```

```
240 n = n + 1
250 IF n = 103 THEN GOTO 300
260 GOTO 220

300 REM ** ENTER DATA **
310 PRINT
320 PRINT "How many reactants";
330 INPUT rxt
340 PRINT
405 FOR main = 1 TO rxt + 1
410 IF main = rxt + 1 THEN GOTO 411 ELSE GOTO 415
411 INPUT "What is the product"; cmp$(main)
412 INPUT "What is the coefficient"; pc
413 GOTO 430
415 PRINT "What is reactant"; main;
420 INPUT cmp$(main)
425 INPUT "What is the coefficient"; moles(main)
430 cl = LEN(cmp$(main))
440 FOR x = 1 TO cl
450 cc$(x) = MID$(cmp$(main), x, 1)
460 NEXT x


600 REM **  CHECK EACH CHARACTER IN COMPOUND **
610 FOR x = 1 TO cl
620 IF ASC(cc$(x)) > 64 AND ASC(cc$(x)) < 91 THEN GOTO 3000
630 IF ASC(cc$(x)) > 96 AND ASC(cc$(x)) < 123 THEN GOTO 3200
640 IF ASC(cc$(x)) > 45 AND ASC(cc$(x)) < 58 THEN GOTO 3300
650 NEXT x
660 IF p = 1 THEN atoms$(cnt) = "1"


800 REM **  CALCULATION  **
810 FOR y = 1 TO cnt
820 FOR x = 1 TO 103
830 IF e$(y) = element$(x) THEN GOTO 870
840 NEXT x
850 NEXT y
860 GOTO 900
870 em(y) = VAL(atoms$(y)) * mmass(x)
880 total = total + em(y)
890 GOTO 840
900 mascmp(main) = total
910 FOR x = 1 TO cnt
920 atoms$(x) = ""
930 NEXT x
```

```
940 p = 0: q = 0: total = 0
950 NEXT main
970 PRINT
975 INPUT "How many grams of product will be made"; gr
985 am = (gr / mascmp(rxt + 1)) / pc


1000 REM ** PRINT RESULTS **
1010 PRINT : PRINT "Reactant", "Exp. Mass", "Molar Mass": PRINT
1020 FOR x = 1 TO main - 2
1030 PRINT cmp$(x), INT(10000 * am * mascmp(x) * moles(x)) / 10000,
mascmp(x)
1040 NEXT x
1050 PRINT
1060 INPUT "Another Compound"; a$
1070 IF LEFT$(a$, 1) = "y" THEN GOTO 110
1080 END


2990 REM ** CAPITAL LETTER ELEMENT **
3000 IF p = 1 THEN GOTO 3010 ELSE GOTO 3030
3010 atoms$(cnt) = "1"
3020 GOTO 3050
3030 IF q = 1 THEN GOTO 3040 ELSE GOTO 3050
3040 atoms$(cnt) = "1"
3050 cnt = cnt + 1
3060 e$(cnt) = e$(cnt) + cc$(x)
3070 p = 1
3080 q = 0
3090 GOTO 650


3200 REM ** LOWER CASE OF ELEMENTS **
3210 e$(cnt) = e$(cnt) + cc$(x)
3220 p = 0
3230 q = 1
3240 GOTO 650


3300 REM ** NUMBER OF ATOMS **
3310 atoms$(cnt) = atoms$(cnt) + cc$(x)
3320 p = 0: q = 0
3330 GOTO 650
```

```
3990 REM ** DATA **
4000 DATA H,1.008,He,4.002602
4010 DATA Li, 6.941, Be, 9.01218, B, 10.811, C, 12.011, N, 14.0067, O,
          15.9994, F, 18.998403, Ne, 20.179

4020 DATA Na, 22.98977, Mg, 24.305, Al, 26.98154, Si, 28.0855, P, 30.97376,
          S, 32.066, Cl, 35.453, Ar, 39.948

4030 DATA K, 39.0943, Ca, 40.078, Sc, 44.95591, Ti, 47.88, V, 50.9415, Cr,
          51.9961, Mn, 54.9380, Fe, 55.847, Co, 58.9332, Ni,55.69, Cu,
          63.546, Zn, 65.39

4040 DATA Ga, 69.723, Ge, 72.59, As, 74.9216, Se, 78.96, Br, 79.904, Kr, 83.80

4050 DATA Rb, 85.4678, Sr, 87.62, Y, 88.9059, Zr, 91.224, Nb, 92.9064, Mo,
          95.94, Tc, 98, Ru, 101.07, Rh, 102.9055, Pd, 106.42, Ag,
          107.8682, Cd, 112.41

4060 DATA In, 114.82, Sn, 118.710, Sb, 121.75, Te, 127.60, I, 126.9045, Xe,
          131.29

4070 DATA Cs, 132.9054, Ba, 137.33, La, 138.9055

4080 DATA Ce, 140.12, Pr, 140.9077, Nd, 144.24, Pm, 145, Sm, 150.36, Eu,
          151.965, Gd, 157.25, Tb, 158.9254, Dy, 162.50, Ho, 164.9304, Er,
          167.26, Tm, 168.9342, Yb, 173.04, Lu, 174.967

4090 DATA Hf, 178.49, Ta, 180.9479, W, 183.85, Re, 186.207, Os, 190.2, Ir,
          192.22, Pt, 195.08, Au, 196.9665, Hg, 200.59

4100 DATA Tl, 204.383, Pb, 207.2, Bi, 208.98037, Po, 209, At, 210, Rn, 222

4110 DATA Fr, 223, Ra, 226.0254, Ac, 227.0278, Th, 232.0381, Pa, 231.0359,
          U, 238.0289, Np, 237.0482, Pu, 244, Am, 243, Cm, 247, Bk, 247,
          Cf, 251, Es, 252, Fm, 257, Md, 258, No, 259, Lr, 260
```

Stephen Kenneth Crossno
Department of Chemistry, Gilbert 153
Oregon State University
Corvallis, OR. 97330

Education

M.S. Materials Chemistry, Oregon State University, June 1997 (GPA 3.00) B.A. Chemistry, Cal. State University San Bernardino, June 1994 (GPA 3.00)

Honors and Awards

Teaching Assistant Award
Oregon State University Chemistry, 1996

Phi Lambda Upsilon, Chemistry Honor Society
Oregon State University, 1996

Outstanding Analytical Chemistry Student, American Chemical Society award to Third Year Undergraduates, California State University San Bernardino, 1993

Presentations and Publications

1. Oral presentation at the 205th national meeting of the American Chemical Society, general papers session, Denver, March 1993

2. S. K. Crossno, L. E. Kalbus, G. Kalbus, "Determinations of Carbon Dioxide by Titration," *Journal of Chemical Education*, **73**, 175-176, (1996).

3. D. A. Keszler, G. Peterson, S. K. Crossno, R. Meltzer, Structure-Property Relationships in VUV Excited Phosphors, *J. of SID*, in press.

4. S. K. Crossno and D. A. Keszler, Structures and Optical Properties in the Borate Family $A_4LnO(BO_3)_3$ (A=Sr, Ca, Mg; Ln=lanthanide), manuscript in preparation.